

---

Report No. K-TRAN: KU-02-1  
FINAL REPORT

**IDENTIFICATION OF FAILURE PREDICTION CRITERIA  
USING ACOUSTIC EMISSION MONITORING AND  
ANALYSIS OF GFRP BRIDGE DECK PANELS**

Richard S. Gostautas

The University of Kansas  
Lawrence, Kansas

July 2007

K-TRAN

A COOPERATIVE TRANSPORTATION RESEARCH PROGRAM  
BETWEEN:

KANSAS DEPARTMENT OF TRANSPORTATION  
KANSAS STATE UNIVERSITY  
UNIVERSITY OF KANSAS



<b>1 Report No.</b> K-TRAN: KU-02-1		<b>2 Government Accession No.</b>		<b>3 Recipient Catalog No.</b>	
<b>4 Title and Subtitle</b> IDENTIFICATION OF FAILURE PREDICTION CRITERIA USING ACOUSTIC EMISSION MONITORING AND ANALYSIS OF GFRP BRIDGE DECK PANELS				<b>5 Report Date</b> July 2007	
				<b>6 Performing Organization Code</b>	
<b>7 Author(s)</b> Richard S. Gostautas				<b>8 Performing Organization Report No.</b>	
<b>9 Performing Organization Name and Address</b> University of Kansas Civil, Environmental & Architectural Engineering Department 1530 West 15th Street, Room 2134 Lawrence, Kansas 66045-7609				<b>10 Work Unit No. (TRAIS)</b>	
				<b>11 Contract or Grant No.</b> C1277	
<b>12 Sponsoring Agency Name and Address</b> Kansas Department of Transportation Bureau of Materials and Research 700 SW Harrison Street Topeka, Kansas 66603-3754				<b>13 Type of Report and Period Covered</b> User's Manual August 2001 - January 2007	
				<b>14 Sponsoring Agency Code</b> RE-0284-01	
<b>15 Supplementary Notes</b> For more information write to address in block 9.					
<b>16 Abstract</b> <p>A total of 6 full-scale glass fiber-reinforced polymer (GFRP) composite bridge deck specimens were tested to study the significance of using acoustic emission (AE) for monitoring and analysis of the structural integrity of the specimens during a predetermined loading profile. The first two specimens varied in width and were loaded to failure and last four specimens were the original specimens that were repaired after failure occurred using an FRP wrap.</p> <p>The objective, through the use of AE monitoring and analysis, is to identify failure prediction criteria and/or a methodology that would provide a determination of the structural integrity of the in-service FRP bridge deck during field inspection. While no codes and standards exist for these types of specimens, current standards developed for FRP tanks and vessels were used as a base reference to determine if current standards could be adopted or if new or additional criteria needed to be established.</p> <p>Real-time monitoring was conducted for each specimen during a standard 3-point bending test. Monitoring typically covered loading up to 80% of the calculated ultimate strength. During monitoring, a selected set of features associated with each AE hit and the associated waveform were recorded in a database for post analysis. The collected data was later analyzed using comparison and intensity analysis, linear location and waveform analysis, accompanied with pattern recognition, to identify series of hits with a particular event. Each event was investigated to determine if the type of damage, such as fiber breakage, matrix cracking, and delamination, could characterize the event. These types of events were the contributing factors to the investigated criteria and the structural performance of the specimens.</p> <p>In post analysis, comparison analysis was performed to observe the Kaiser Effect and the calculation of a Felicity Ratio when the Kaiser Effect broke down. For the original specimens, the Felicity Ratio fell within expected values observed from previous work, while the repaired specimens, using an external FRP wrap, were generally higher than the typically accepted value of 0.85.</p> <p>The second type of post analysis, linear location, was performed to pinpoint the location along the axis of the specimen in which the majority of the events occurred. In the case of the original specimens, visual inspection was difficult as the majority of the damage of the specimen occurred at the inner core. While there is some associated stress redistribution that leads to delamination of the outer flutes from the top and bottom face panels, this was the only visually observable change for the original specimens. Thus, linear location becomes an important tool for the location and isolation of major damage before reaching catastrophic failure. The failure mode of the repaired specimens was restricted due to the external wrap, and provided a visual cue of damage.</p> <p>The third type of analysis, waveform analysis using pattern recognition, appears promising in identifying each type of damage characteristic and training a neural network to classify incoming waveforms. This damaged based characterization could be useful for in-field service inspection. However, further investigation is needed for verification before using this form of classification.</p>					
<b>17 Key Words</b> Bridge, Computer Program, Hydraulics, Manual, Piers and Scour			<b>18 Distribution Statement</b> No restrictions. This document is available to the public through the National Technical Information Service, Springfield, Virginia 22161		
<b>19 Security Classification (of this report)</b> Unclassified		<b>20 Security Classification (of this page)</b> Unclassified		<b>21 No. of pages</b> 85	<b>22 Price</b>



# **IDENTIFICATION OF FAILURE PREDICTION CRITERIA USING ACOUSTIC EMISSION MONITORING AND ANALYSIS OF GFRP BRIDGE DECK PANELS**

**Final Report**

Prepared by  
Richard S. Gostautas

A Report on Research Sponsored By

THE KANSAS DEPARTMENT OF TRANSPORTATION  
TOPEKA, KANSAS

and

UNIVERSITY OF KANSAS CENTER FOR RESEARCH, INC.  
LAWRENCE, KANSAS

March 2007

© Copyright 2007, **Kansas Department of Transportation**

## **PREFACE**

The Kansas Department of Transportation's (KDOT) Kansas Transportation Research and New-Developments (K-TRAN) Research Program funded this research project. It is an ongoing, cooperative and comprehensive research program addressing transportation needs of the state of Kansas utilizing academic and research resources from KDOT, Kansas State University and the University of Kansas. Transportation professionals in KDOT and the universities jointly develop the projects included in the research program.

## **NOTICE**

The authors and the state of Kansas do not endorse products or manufacturers. Trade and manufacturers names appear herein solely because they are considered essential to the object of this report.

This information is available in alternative accessible formats. To obtain an alternative format, contact the Office of Transportation Information, Kansas Department of Transportation, 700 SW Harrison Street, Topeka, Kansas 66603-3754 or phone (785) 296-3585 (Voice) (TDD).

## **DISCLAIMER**

The contents of this report reflect the views of the authors who are responsible for the facts and accuracy of the data presented herein. The contents do not necessarily reflect the views or the policies of the state of Kansas. This report does not constitute a standard, specification or regulation.

## **ABSTRACT**

A total of 6 full-scale glass fiber-reinforced polymer (GFRP) composite bridge deck specimens were tested to study the significance of using acoustic emission (AE) for monitoring and analysis of the structural integrity of the specimens during a predetermined loading profile. The first two specimens varied in width and were loaded to failure and last four specimens were the original specimens that were repaired after failure occurred using an FRP wrap.

The objective, through the use of AE monitoring and analysis, is to identify failure prediction criteria and/or a methodology that would provide a determination of the structural integrity of the in-service FRP bridge deck during field inspection. While no codes and standards exist for these types of specimens, current standards developed for FRP tanks and vessels were used as a base reference to determine if current standards could be adopted or if new or additional criteria needed to be established.

Real-time monitoring was conducted for each specimen during a standard 3-point bending test. Monitoring typically covered loading up to 80% of the calculated ultimate strength. During monitoring, a selected set of features associated with each AE hit and the associated waveform were recorded in a database for post analysis. The collected data was later analyzed using comparison and intensity analysis, linear location and waveform analysis, accompanied with pattern recognition, to identify series of hits with a particular event. Each event was investigated to determine if the type of damage, such as fiber breakage, matrix cracking, and delamination, could characterize the event. These types of events were the contributing factors to the investigated criteria and the structural performance of the specimens.

In post analysis, comparison analysis was performed to observe the Kaiser Effect and the calculation of a Felicity Ratio when the Kaiser Effect broke down. For the original specimens, the Felicity Ratio fell within expected values observed from previous work, while the repaired specimens, using an external FRP wrap, were generally higher than the typically accepted value of 0.85.

The second type of post analysis, linear location, was performed to pinpoint the location along the axis of the specimen in which the majority of the events occurred. In the case of the original specimens, visual inspection was difficult as the majority of the damage of the specimen occurred at the inner core. While there is some associated stress redistribution that leads to delamination of the outer flutes from the top and bottom face panels, this was the only visually observable change for the original specimens. Thus, linear location becomes an important tool for the location and isolation of major damage before reaching catastrophic failure. The failure mode of the repaired specimens was restricted due to the external wrap, and provided a visual cue of damage.

The third type of analysis, waveform analysis using pattern recognition, appears promising in identifying each type of damage characteristic and training a neural network to classify incoming waveforms. This damaged based characterization could be useful for in-field service inspection. However, further investigation is needed for verification before using this form of classification.

**Keywords:** acoustic emission (AE); fiber-reinforced plastics (FRP); composite sandwich panels; comparison analysis; intensity analysis; linear location; waveform analysis; neural network; bridge inspection; damage assessment.

## **ACKNOWLEDGEMENTS**

I wish to thank the following people for their assistance and support in helping me complete this thesis:

Assistant Professor Guillermo Ramirez, Dept. of Civil Engineering, graduate advisor and chairmen of my committee, for his constant support, guidance, experience and appreciation in working with composites. Mr. Adrian Pollock and Mark Carlos of Physical Acoustics Corporation for their commitment to teaching and assistance in the use of acoustic emission equipment and software. Associate Professor Bob Peterman of Kansas State University and Research Development Engineer Dave Meggers of the Kansas Department of Transportation, for their invitation to work with them on this project. Mr. Jerry Plunkett, Kansas Structural Composites Inc., for providing the FRP honeycomb sandwich panels used in this study.

Finally, I wish to thank my wife, parents, family members and friends for their love, encouragement, support and understanding for the time it took away from them to complete this work.

Funding for this research was provided by project KAN26280.

# TABLE OF CONTENTS

<b>ABSTRACT .....</b>	<b>ii</b>
<b>ACKNOWLEDGEMENTS .....</b>	<b>v</b>
<b>TABLE OF CONTENTS.....</b>	<b>vi</b>
<b>LIST OF TABLES .....</b>	<b>viii</b>
<b>LIST OF FIGURES.....</b>	<b>ix</b>
<b>CHAPTER 1 - INTRODUCTION .....</b>	<b>1</b>
<b>1.1 Status of the nation’s bridges .....</b>	<b>1</b>
<b>1.2 Composites – an alternative use material .....</b>	<b>2</b>
<b>1.3 Previous work.....</b>	<b>5</b>
<b>1.4 Inspection using acoustic emission .....</b>	<b>7</b>
<b>1.5 Waveform signature analysis using pattern recognition .....</b>	<b>12</b>
<b>1.6 Objective and Scope .....</b>	<b>17</b>
<b>CHAPTER 2 - EXPERIMENTAL WORK .....</b>	<b>18</b>
<b>2.1 Experimental Background .....</b>	<b>18</b>
<b>2.2 AE Software and Data Acquisition (DAQ) setup .....</b>	<b>18</b>
<b>2.3 AE Sensors and setup locations.....</b>	<b>27</b>
<b>2.4 GFRP Bridge deck panel manufacturing and specifications.....</b>	<b>28</b>
<b>2.4.1 Panel Manufacturing and Specifications .....</b>	<b>29</b>
<b>CHAPTER 3 – RESULTS AND EVALUATION .....</b>	<b>33</b>
<b>3.1 Test Case: A30-Original .....</b>	<b>33</b>
<b>3.1.1 Comparison Analysis .....</b>	<b>35</b>
<b>3.1.2 Intensity Analysis .....</b>	<b>41</b>
<b>3.1.3 Waveform signature analysis .....</b>	<b>48</b>
<b>CHAPTER 4 – SUMMARY AND CONCLUSIONS .....</b>	<b>64</b>

<b>4.1</b>	<b>Summary .....</b>	<b>64</b>
<b>4.2</b>	<b>Conclusions .....</b>	<b>64</b>
<b>4.3</b>	<b>Future Work .....</b>	<b>66</b>
	<b>REFERENCES.....</b>	<b>68</b>
	<b>Appendix A .....</b>	<b>Error! Bookmark not defined.</b>
	<b>Appendix B .....</b>	<b>Error! Bookmark not defined.</b>

## LIST OF TABLES

Table 2.1: Constituent Material Properties (for Polyester Resin).....	31
Table 3.1: Summary of comparison analysis results for all panels.....	46
Table 3.2: Number of patterns/hits in each class .....	56
Table 3.3: Feature statistics for selected classes.....	58
Table 3.4: Feature discriminant analysis results .....	60
Table 3.5: Number of patterns/hits in each class .....	61
Table 3.6: Feature statistics for selected classes.....	61

## LIST OF FIGURES

Figure 1.1: Corrosion of steel superstructure .....	2
Figure 1.2: Placement of composite panels .....	3
Figure 1.3: Typical Load Profile.....	9
Figure 1.4: AE waveform characteristics .....	13
Figure 2.5: Waveform display for screen #1 .....	24
Figure 2.6: Typical sensor locations .....	26
Figure 2.7: Sensor instrumentation of A18-repaired panel .....	29
Figure 3.5: Distribution plots of recorded hits .....	38
Figure 3.6: Plot of cumulative signal strength in time for all channels .....	39
Figure 3.7: Cross plot of duration versus amplitude .....	40
Figure 3.8: Plot of historic index and cumulative signal strength .....	42
Figure 3.9: Plot of severity versus cumulative signal strength.....	43
Figure 3.10: Plot of severity versus load profile.....	44
Figure 3.11: Plot of amplitude versus time .....	47
Figure 3.12: Debonding of wrap along edges.....	48
Figure 3.13: Noesis plot of amplitude versus time.....	50
Figure 3.14: Feature correlation hierarchy .....	51
Figure 3.15: Noesis graph with normalization applied .....	52
Figure 3.16: Plot of data along PCA 0 .....	53
Figure 3.16: Plot of data along PCA 0 .....	53
Figure 3.17: Plot of data along PCA 1 .....	53
Figure 3.18: Plot of data along PCA 2 .....	54
Figure 3.19: Plot of data along PCA 3 .....	54
Figure 3.20: Clustering analysis results – PCA 0 .....	56
Figure 3.21: Applied clustering method to original data.....	62

# CHAPTER 1 - INTRODUCTION

## 1.1 Status of the nation's bridges

The Federal Highway Administration created the National Bridge Inventory database as part of the National Bridge Inspection Program. This inventory is compiled in a database and information can be found online from 1992 to the present. In 1992 there were 199,090 bridges (46%) in the United States that were rated as structurally deficient or functionally obsolete (FHWA 2003). Bridges rated as structurally deficient were either closed or restricted to light vehicles due to the deteriorating structural components, which may require speed and weight restrictions. Bridges rated as functionally obsolete were those that had older design features and though not unsafe for vehicles, could not safely accommodate current volume, sizes or weights of traffic (ASCE 2003).

As of 2002, there were only 163,010 bridges with the same rating, a decrease of 18%. Part of this decrease can be contributed to the funding provided by the Transportation Equity Act for the 21<sup>st</sup> Century (TEA-21) (FHWA 2003). Later the FHWA released report FHWA-RD-01-156 titled "Corrosion Costs and Preventative Strategies in the United States" which was initiated by the NACE International – The Corrosion Society and mandated by congress as part of TEA-21. This 2-year study reviewed the direct costs associated with metallic corrosion. The report covered 5 major sector categories broken into 26 sectors. According to this study, it is estimated that \$8.3 billion is spent on highway bridges, including \$3.8 billion to replace deficient bridges over the next 10 years, \$2 billion on maintenance and capital costs of concrete decks and \$2 billion for concrete substructures. This part of the study also estimated the

indirect cost to the user would be as high as 10 times that of the direct corrosion cost due to traffic delays and lost productivity (FHWA, USDOT 2002).

While the percentage of deficient and obsolete bridges has decreased, despite the rising costs of maintenance, the ASCE 2003 Progress Report clarifies that current funding trends of state DOT's could hamper progress on addressing future bridge deficiencies and once again, federal action will be needed to prevent deterioration. In the face of funding shortfalls, states and owners are now beginning to look at technology for alternative use materials for bridge replacement, repair and rehabilitation.

## 1.2 Composites – an alternative use material

Assistance in the use of new materials came under TEA-21 legislation with a new program called the Innovative Bridge Research and Construction Program (IBRC). The primary goal of this program was the development and demonstration of new, cost-effective applications for highway bridges using alternative materials. In the past six years, the program has funded 246 proposals using high performance materials. Of these, 127 proposals are constructed using FRP composites for concepts in bridge



**Figure 1.1: Corrosion of steel superstructure**

design and construction (Tang, FHWA 2003). The primary applications of FRP in bridge applications include hybrid construction (FRP reinforcement), bridge strengthening, repair and seismic retrofit of columns and bridge deck systems. For bridge deck systems, the two primary types of

system seen today are sandwich construction and adhesively bonded pultruded shapes. Part of the focus of this study is on the performance and evaluation of FRP bridge decks using sandwich construction.

Sandwich construction is widely used in aerospace and automotive industries where stiffness and strength requirements with minimal weight must be met. This type of construction has provided a broad base of examples for review and future design in the use of civil engineering applications. Composites are gaining ground due to their high strength, corrosion resistance, lightweight form, high strength-to weight ratio, ease of erection, year-round construction, short project time delivery and the ability to tailor the material to meet the needs of the bridge owner. Though considered relatively new to the U.S., FRP bridge applications have been widely used in Japan and Europe (FHWA, USDOT 1997).

Aided by the success of several completed FRP bridge deck projects (FHWA 2003), one such successful implementation is the Bentley Creek Bridge in Chemung County in the state of New York. This project was the first application of a FRP deck for



**Figure 1.2: Placement of composite panels**

a truss bridge on a state highway system.

This steel truss bridge was built in 1940 and considered a good case for replacement due to its age, structural condition and the 14-ton weight restriction.

The project was completed over the course of two construction seasons. The old deck

was removed and the supporting steel was

examined for corrosion and section loss (Figure 1.1). Once the repairs were made, a temporary steel grate deck was installed until the following season. At this time, the temporary deck was removed and replaced with an FRP deck, which took less than a month to complete. A 32 psf FRP deck (6 panels covering a 25' x 141' area) replaced the original 170 psf concrete deck and wearing surface that had been continuously added over the years for a total of 265 tons of dead load being removed (Figure 1.2). The use of FRP almost doubled the bridge load rating and met the L/800 deflection requirement. The truss rating before replacement had an inventory load rating of H17 (17 tons) and operating load rating of H30 (30 tons). After replacement, the inventory load rating increased to H55 (55 tons) and operating load rating of H85 (85 tons). Additional modifications included a FRP sidewalk replacement (32 ton dead load reduction), and FRP filler panels between the deck and sidewalk to protect the bottom chord of steel truss from environmental intrusion. This FRP deck replacement is believed to extend the service life of the bridge approximately 30 years. In most cases, for a bridge near the end of its service life, the entire structure would have to be replaced and tends to be expensive. However, the cost of replacement using the FRP deck was \$876,000 compared to an estimated cost of \$2.3 million for designing and construction of a similar replacement bridge, thus providing a substantial cost benefit. A summary of benefits with this project were the reduction in cost vs. replacement, improved load ratings, reduction in environmental impact to surrounding habitat, reduced construction time, service-life extension and minimal impact to users (FHWA/NY 2000).

These are just a few of the beneficial characteristics that make FRP composites a highly desirable material alternative. However, there are several factors that have prohibited FRP technology from being widely accepted. Several problems have been identified by the Committee of Structural Fiber Reinforced Plastics (A2C07) of TRB. These problems address field inspection, maintenance and repair of existing FRP bridge decks and superstructures. According to their review, inspection and monitoring of existing FRP structures has varied widely. This includes no monitoring, to experimental nondestructive evaluation (NDE) techniques, to load testing and periodic visual inspection. Of main concern is the inability to obtain performance data of existing structures. While reporting has been occurring in several publications, there is no standard format currently in place, which hampers the abilities of interested states and bridge owners to compare one project to another. Another factor is that of the all-composite bridges found in the U.S., they were all built starting in the 1990's. Some repairs and modifications have been made to correct construction problems, but were primarily handled by the parties involved in the original construction and have thusly led to a lack of developed routine maintenance practices (TRB 2003). Additional disadvantages include initial manufacturing costs, aerodynamic instability, global and local buckling, limited joint technology, and the consistency of material properties and fabrication.

### **1.3 Previous work**

Though there is currently a lack of standards and design codes regarding the performance and structural integrity of FRP bridge decks for in-service field inspection, this study analyzed the results of using long standing NDE techniques that have been

used in a wide variety of industrial inspection applications. These techniques include inspection of railroad tank cars, pressure vessels, aircraft, welds and concrete structures, to name a few.

In 1978 the committee on Acoustic Emission from Reinforced Plastics (CARP) was formed under the support of The Society of the Plastics Industry (SPI). The initial objective of this committee was the development of test methods of FRP vessels and piping system using acoustic emission (AE). Over the first 10 years of existence, CARP gained valuable experience in testing of FRP tanks, pressure vessels, and other structural members through the cooperation of fabricators, chemical companies, material suppliers, instrument manufactures as well as academic and research institutions. During this time, it is estimated that CARP tested approximately 7,000 FRP tanks and vessels, and 10,000 pipe tests (Blessing, Conlisk, Fowler 1989). This accumulation of data allowed for extensive research and evaluation of test results to help identify and develop a set of evaluation criteria using AE. Several programs were initiated during that time that went on to support the major impact that AE can have on the structural integrity, performance and safety of FRP members. All this work led to the "CARP Recommended Practice for Tanks/Vessels" which was published in January of 1982, and became the foundation for the SPI/CARP recommended practice for piping systems, The American Society for Testing Materials (ASTM) standards (ASTM 1985, 1986) and the American Society of Mechanical Engineers (ASME) codes (ASME 1985, 1986) as well as additional procedures (Blessing et al. 1989, AAR 1993, Fowler 1993). Overall, the development of these standards led acoustic emission, a NDE technique, to

the forefront of recommend practice and provided a major impact to performance evaluation.

#### **1.4 Inspection using acoustic emission**

Acoustic emission may be defined as a transient sound wave that is generated by a short, rapid release of energy, in the form of an elastic wave (signal), produced by the movement of a dislocation or change in the structural integrity of the material within a specimen. This local material change in the structural integrity of the material, that gives rise to an acoustic emission signal, is known as an event. An event can be further characterized by the type of change and may be related to fiber breakage, matrix cracking, and delamination. Additional factors that may appear as events but are not related to changes in the structural integrity are mechanical rubbing, and electromagnetic interference. Transducers are coupled to the surface of the material can then detect these acoustic emission events passively. This monitoring may be considered “global” in nature as it allows the investigator to get a bigger picture of the overall performance of the specimen without requiring access to every part of the structure. The properties of the acoustic emission signals are then collected and converted into records by an AE acquisition system that stores this information as a hit in a data set. According to most standards, the properties of interest include the location of the hit (by channel), time of occurrence, duration, maximum amplitude, and energy and signal strength of the waveform generated by the event (Bray, Stanley 1997). A ‘hit’ is a signal received by an AE sensor and recorded by the AE system. An ‘event’ corresponds to the physical phenomenon that produced the signal(s).

Since there are no codes or standards available for the evaluation of FRP bridge deck panels, this study used previously established approaches from the investigation of failure criteria. Traditionally, two different approaches, comparison analysis (Blessing, Conlisk, Fowler 1989) and intensity analysis (Blessing, Fowler, Strauser 1992), have been used for evaluation. Comparison analysis is considered a trend approach that evaluates the peak amplitudes of the recorded signals in time with its corresponding cumulative signal strength. This type of analysis allows for the initial characterization of the events, a check of the Kaiser Effect, a check of the Felicity Effect and determination of a Felicity Ratio when the Kaiser Effect was no longer valid.

The Kaiser Effect is a case of the indication of prior loading of a specimen. This effect states that if a sample is loaded, unloaded and then reloaded under the same conditions, no acoustic emission events should be detected until the previous load peak is achieved or passed. This condition considered to be satisfied if no permanent damage within the specimen has occurred. Thus, when there is an occurrence of emissions at a load below the previous maximum load, the Kaiser effect is no longer valid, and this condition is known as the Felicity effect. The significance of this effect and its related damaged is defined by a Felicity Ratio (FR). This ratio is defined as:

$$Felicity\ Ratio = \frac{\text{load at which AE events are first generated upon reloading}}{\text{previously applied maximum load}} \quad (1)$$

A FR of 1 or greater can be interpreted as showing that no damage in the structure has occurred since the last AE inspection. However, a decreasing FR in later inspections may be indicative of cumulative, permanent damage and may result in the rejection and removal of the specimen (Bray, Stanley 1997). In the CARP

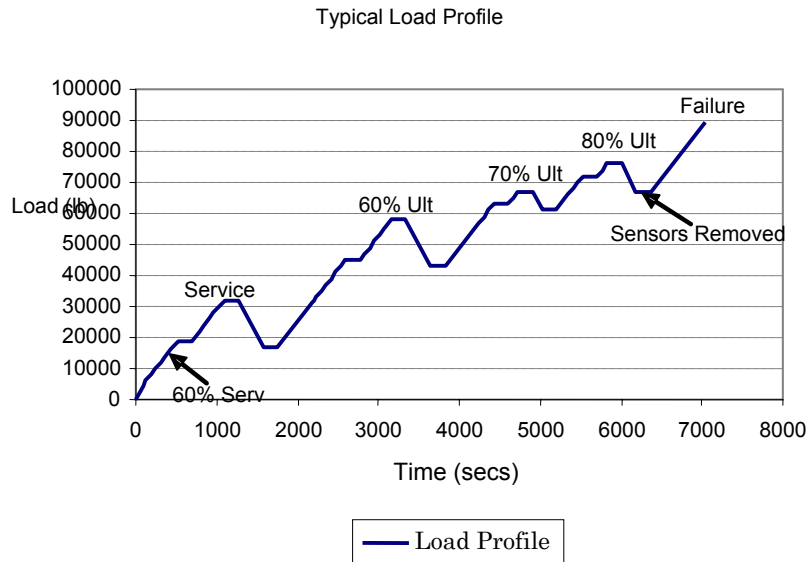


**Figure 1.3: Typical Load Profile**

Recommended Practice for Tanks and Vessels, the value of the FR is one of four acceptance criteria used as part of the criteria index method for evaluating the deterioration of the vessel. Based on these results, a FR close to 0.85 or less has been associated with the onset of permanent damage in pressure vessels, and the lower the value the more serious the defect. However, there are situations in which large amounts of emission may not necessarily indicate structural damage. Such cases have occurred during initial loading in which excess surface resin may crack and result in a large amount of AE activity. Therefore, the loading profile seen in Figure 1.3 was adopted to allow for the determination of the Kaiser Effect and Felicity Ratio through each step of the loading process.

Both of these effects provide insight into the behavior of the specimen under loading. Since this study is of a different nature, it becomes important in determining whether this value can be applied to composite bridge deck systems, or if a new set of evaluation criteria is needed.

The second adopted approach is known as intensity analysis. Intensity analysis is known as a statistical approach and is a method of measuring the structural significance of an event by calculating two values called historic index (HI) and severity (Sr) and evaluating their change in time for each individual channel. Calculation of the historic index is an analytical method of estimating the changes of slope in the cumulative signal strength against time by comparing the signal strength of the most recent hits to all the hits for that channel. The use of historic index has been found to determine the AE knee in the cumulative signal strength curve in time. Above the knee, the historic index tends to decrease until the next AE knee is reached and has been shown to be important in identifying possible damage mechanism. After the next knee, the historic index will continue to decline until the onset of failure, at which point it increases to a maximum. However, in the case of FRP composites, more than one knee will be seen, but it does not necessarily guarantee that a point of failure is occurring within the specimen at that time. Since past tests have shown a rapid fluctuation in the historic index value for the first 100 hits due to cracking of excessive matrix material under initial loading, the first 100 hits are discarded. The calculation of the historic index (HI) is as follows (Blessing, Fowler, Strauser 1992):

$$H(I) = \frac{N}{N-K} * \left( \frac{\sum_{i=K+1}^N S_{oi}}{\sum_{i=1}^N S_{oi}} \right) \quad (2)$$

# of hits (N)	K
≤ 100	Not applicable
101 to 500	0.8*N
> 500	N-100

Where:

N ~ Number of hits up to and including time (t)

S<sub>oi</sub> ~ Signal strength of the i<sup>th</sup> event

K ~ empirically derived constant based on material type (composites) and number of hits

Severity is defined as the average signal strength for a given number of events (J) having the largest value of signal strength. Severity can only increase or remain

constant as the load is increased. A rapid increase in severity is typically associated with the onset of structural damage and the onset of emissions for calculation of the Felicity Ratio as previous discussed. As damage continues to become more serious, there will be a continued increase in the severity, but at a reduced rate. The calculation of Severity ( $S_r$ ) for composites is defined as follows (Blessing, Fowler, Strauser 1992):

$$S_r = \frac{1}{J} * \left( \sum_{i=1}^{i=J} S_{om} \right) \quad (3)$$

# of hits (N)	J
< 20	Not applicable
≥ 20	20

Where:

$S_{om}$  ~ is the signal strength of the  $m^{\text{th}}$  hit, where the ordering of  $m$  is based on magnitude of signal strength.

J ~ empirically derived constant based on material type (composites) and number of hits

Thus, through the use of intensity analysis, historic index and severity provide useful tools for possible identification of the onset of damage mechanisms and a measure of the damage mechanisms respectively. However, the calculation of each will depend on the type of material (metals, composites), and must be made on data acquired during the load cycle which may include load holds. A final step for determining the intensity of an emission source can developed by plotting the maximum values of severity and historic index on a log-log chart for each test. This chart can then be divided into intensity zones which would indicate the structural significance of the emissions. Intensity values of high structural significance will plot toward the top right-hand corner of the chart while values of less significance near the bottom left. Such charts would ease the evaluation of the panels for in-service inspection. However, due

to the limited number of specimens available during testing, intensity zones could not be clearly identified or established for this study.

### **1.5 Waveform signature analysis using pattern recognition**

While identification of failure mechanisms is important, the ability to characterize each type of failure mechanism would provide a better evaluation of the panels and would easily establish acceptance or removal criteria for field use. In the early 1980's, CARP conducted a study to identify and characterize AE failure mechanisms in FRP composites (Blessing, Conlisk, Fowler, 1989). This study consisted in testing FRP specimens that contained known defects and identifying the AE characteristics for each defect. This study also included a group of experienced field inspectors, which compiled a list of AE characteristics that they use for identification of a particular defect. It was found that each inspector was able to accurately identify specific damage mechanisms of the known defects. This led to the suggestion of using pattern recognition and has been partially successful in later studies (Ohtsu, Ono, 1987). By using pattern recognition, it becomes possible to create a neural network that uses adaptive learning behavior to comparing identified patterns in the waveform from previous case histories and then classifying the waveform by the type of failure mechanism.

As previously mentioned, composites have several failure mechanisms such as matrix cracking, fiber breakage, debonding and delamination. However, for pattern recognition of neural networks to be successful, AE emission parameters need to be carefully selected. Traditionally, AE parameters such as amplitude, duration, counts, and rise time have been used (Figure 1.4). For this study, a software program called "Noesis" was used. Noesis is an integrated neural network and pattern recognition

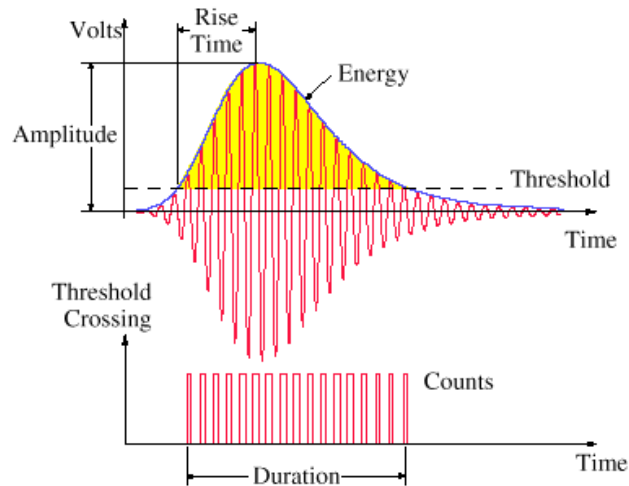


**Figure 1.4: AE waveform characteristics**

package specifically designed for optimization for the analysis of AE data. Noesis uses unsupervised pattern recognition (UPR) techniques to determine similar classes within AE signals. These classes use the AE waveform parameters to try to identify and characterize the type of failure mechanisms that occurred during testing of the FRP panels. Based upon these classes, Noesis allows the training of supervised pattern recognition algorithms so that the classification of each failure mechanism can be applied to new, unknown data.

Since there are no previous identified classes trained for these types of FRP panels, the unsupervised pattern technique is applied first. To begin this type of analysis, the original data and recorded waveforms from the monitoring procedure is loaded into the program and called the “As Loaded” data set. Once loaded, similar graphs used during monitoring can be created in order to view and compare the current data set (e.g. amplitude versus time graph). From these graphs the user can view each hit, and associated waveform by double clicking on the hit of interest. To begin manipulating the data and processing it for analysis, there are several steps that are performed. The first step is to switch from the “As Loaded” data set to the “Working

Copy” data set. The working copy is the pre-processed form of the data in which the unsupervised pattern recognition method is applied. The second step is to extract additional waveform features not originally recorded during testing using the built-in function called “Feature Extraction”. This function allows for a total of 22 additional waveform parameters to be extracted from the original data set, which may be useful in improving pattern recognition or investigating additional criteria. Also included in this function is the ability to delete waveforms below the set threshold or delete records with no associated waveform. However, deleting records with no associated waveform should be used carefully as it may result in the removal of valid data from your working data set. Missing waveforms can occur at critical points in testing when a large amount of data is being received, but due to the limitations of the hardware and software all waveforms may not be recorded. The user may then view the new set data, with the new extracted features, and if desired, may save this data into a new data set for additional analysis.

As it is common practice to investigate the correlation between various waveform parameters, a built-in function called “Correlation Matrices” uses hierarchical clustering that is applied to the data correlation matrix and then outputs the results in the form of a dendrogram. A horizontal line in the dendrogram connects the two most correlated waveform features that result in a new cluster. The correlation matrix is then updated and the process continues until all features are merged into a single group.

The next step in analysis is to begin preprocessing the data. Since the original features and extracted features are not necessarily measured in the same range or units, the data needs to be normalized so that the values of each feature attain the

same weight. Once this has been done, each of the selected features is given a calculated eigenvalue, which represents the importance of each feature selected. The previously mentioned correlation matrices are now applied to the normalized data and a new set of eigenvalues are calculated. The final step of pre-processing is to create a projection of the data to their principal components axes. This part of the analysis projects the data on a set of artificial orthogonal axes in which maximum variance is achieved. The variance of the projected data on each new axis equals the corresponding eigenvalue and each axis corresponds to a real feature. To determine how well the new axes will fit the data, the function Degree-Of-Fit (DOF) can be applied. Based upon the new eigenvalues the user chooses which features to use for analysis. This not only reduces the number of features for analysis but also provides a cleaner data set.

Now that pre-processing is completed, the next step is to begin clustering the data. The clustering methods available are unsupervised algorithms that use similar criteria to perform a partition of the data into classes (also called clusters). Some of the available methods include Max-Min Distance, K-Means, Forgy, Cluster-Seeking and a few others. Each method has its own strategy for determining clusters in which the desired result for each cluster created will correspond to a failure mechanism, such as fiber-breakage, matrix cracking or debonding. This study evaluated four different clustering techniques to try and identify which method provided the greatest separation in the data.

Once the clustering method is completed, each class is inspected. The user can then return to the statistics menu to view the feature, data and class statistics. The combination of feature and class statistics is used to evaluate clustering results.

Additionally, the calculation of the number of hits per class helps identify small classes and assist in the decision on whether to merge the class with another class. The final tool used is called “Feature Discriminant Statistics” in which each feature is given three evaluation criteria called Wilk’s, Rij and Tou. Of the three, Rij and Tou are heuristic. Each criteria value is calculated using each selected waveform feature independently. Smaller values for Wilk’s and Rij indicate higher discrimination efficiency for that feature where a higher Tou value indicates higher discrimination. Therefore, the most efficient features can be identified so that better discrimination between the classes and better classification will result. Once satisfied with the results, each class is labeled and training of the data set for use in supervised pattern recognition begins.

For training, two new data sets are created for training supervised methods. Each set is a subset of the main data set and contains all pre-processing and classification information. The first set is the “training data set” which contains the training examples that will be used to train the method and the “testing data set” will contain the records to be used to test the trained method as a verification of adequate training. The schemes used to create the two new data sets are known as a strategy. The testing strategy used was a random half technique in which half of the main set data is randomly picked and used for testing with the other half used for training. Five training strategies are available for use with the selected supervised method. Several supervised methods, such as the k-Nearest Neighbor Classifier (k-NNC), which uses the active supervised method to classify the unknown pattern by assigning it to the class label most frequently occurring among the k nearest samples, Linear Classifier and BP (Back Propagation) Neural Network strategies are available within Noesis. Once the training strategy is

selected and the supervised method applied, Noesis will present the results of the training method based on the number of misclassified records along with an error percentage. This process is continued until the desired error percentage is met in which the method is then saved so that it can be applied later on new, unknown data that has been collected from similar specimens.

## **1.6 Objective and Scope**

The primary objectives of this research are:

1. To evaluate the failure modes and compare the performances of the original and repaired specimens,
2. To examine the performance of the structural interfaces,
3. To characterize the events in relation to the damage mechanism,
4. The establishment of failure predication criteria or a methodology that would provide a determination of the structural integrity of the decks,
5. Provide guidelines and recommended procedures for field inspections of in-service FRP bridge decks.

## **CHAPTER 2 - EXPERIMENTAL WORK**

### **2.1 Experimental Background**

The work for this study was on the structural performance and evaluation of six full-scale GFRP bridge deck specimens, two original manufactured panels and four repaired panels. The research team from Kansas State University handled the first part of the study and contained three objectives. The first objective was to evaluate the specimens having the same face and core thickness but varying in width in order to study the effect of width-to-depth ratio regarding flexural properties. The second objective was to determine an analytical expression to estimate the flexural and shear stiffness of the honeycomb structure. And the third objective was to evaluate analytically and experimentally a repair technique using external FRP wraps. The research team from the University of Kansas handled the second part of the study. This portion of the study used the nondestructive technique known as acoustic emission to monitor the structural changes of the panels during testing. The first objective was to observe the incoming data during AE monitoring to determine if there were any observable patterns that could serve as a benchmark for failure. The second objective was to perform a comparison and statistical analysis of the AE waveform parameters to determine if the data could be characterized by damage type, and whether failure modes or failure prediction criteria could be identified. And the final objective was to use the previous results to provide a methodology that could be used for in-service field inspection.

### **2.2 AE Software and Data Acquisition (DAQ) setup**

The equipment used in the collection of the AE parameters included an 8-channel Data Acquisition (DAQ) system, AE-DAQ software and five to six AE sensors

(transducers). 'Mistras' is the software used for data acquisition (waveform recording) and is a product of Physical Acoustics Corporation (PAC). A simple graphical user interface (GUI) provides a user-friendly environment for setting up the software for monitoring (Figure 2-1). From the menu, 'Test Setup' is used to select all hardware settings for monitoring process. 'Title' allows you to identify each test and appears at the top of the 'hit data set'. In the 'Hardware' menu, the appropriate numbers of channels are setup for each specimen. Each channel has the following parameters: Threshold; db

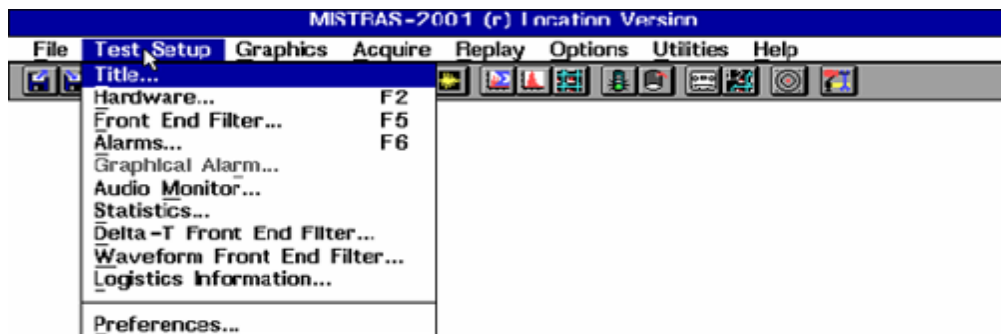


**Figure 2.1: User interface for 'Mistras'**

(decibel); Pre-Amp Gain (db); Sample Rate; Filter (kHz); Pre-Trigger ( $\mu$ s) and Hit Length (k). The fixed threshold defines the minimum decibel level of incoming AE signals that will be recorded by the software. Thus any AE signal below the set threshold will be ignored. The 'pre-amp gain' corresponds to the 2/4/6 preamplifier hardware connected to each channel boosts the incoming voltage of the signal by the designated amount. For a 40 db pre-amp gain, the voltage signal is boosted by 100. The 'sample rate' is that rate at which the PCI DSP-4 board samples waveforms on a per second basis. The 'sample rate' was set to 4 MHz which means that 1 waveform sample is record every  $\frac{1}{4}$   $\mu$ sec. In order to try and eliminate back ground noise, the 'Filter' setting allows for a range of frequencies that will be passed by the preamplifier. These tests used a 'low'

filter of 10 kHz and a 'high' filter setting of 1200 kHz. The 'pre-trigger' value tells the hardware how long to record (in  $\mu\text{sec.}$ ) before the point at which the threshold is exceeded (trigger point). The 'hit length' defines the size of the waveform that is recorded. For these tests, a 4 MHz sampling rate with a 12 k hit length will allow up to 3072  $\mu\text{sec.}$  of data for recording and helps ensure that the entire waveform is recorded.

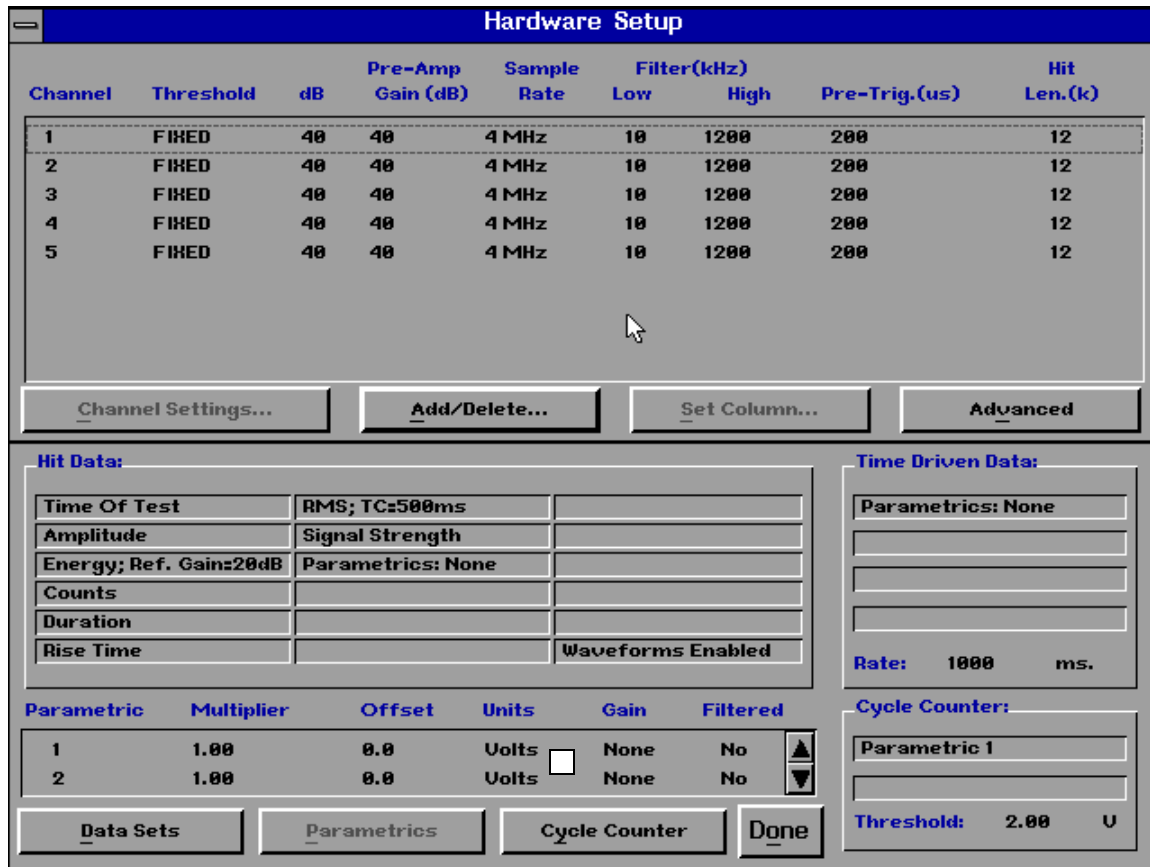


Figure 2.2: User interface for hardware setup

Figure 2-2 shows the typical settings used for each test. As can be seen from Figure 2-2, the software allows for parametric data, such as information from a load cell, to be taken during monitoring. For the purpose of AE monitoring, a special loading profile was designed to assess the AE signature characteristics such as the Kaiser Effect and Felicity ratio. This loading profile contained a series of increasing load rate, load hold, and load drops. The loading scheme was programmed into the load control and was

performed automatically. All loading information was recorded by hand and thusly a parametric setup was not required for 'Mistras'.

Under the 'Advanced' button, three additional parameters known as 'peak definition time (PDT)', 'hit definition time (HDT)' and 'hit lockout time (HLT)' which are timing parameters of the signal measurement process. The PDT helps to ensure that the correct identification of the signal peak. If the PDT is set too short, a high velocity, low-amplitude precursor of an incoming waveform can lead to a false measurement for the rise time. The setting of the HDT allows the reporting of an AE signal as one and only one hit by determining the end of the hit which will stop the measurement process and record the parameters of the signal in the data set. The HDT needs to be set long enough so that it will span over an interval in which the signal to be measured falls below the set threshold. Otherwise, an improper setting may cause the main wave to be treated as separate hits. PAC recommends that the HDT setting be at least twice as long as the PDT. The function of the final setting HLT, is to avoid measuring parts of the signal which may include reflections or late arrival parts. This allows for clean measurement of the main signal and a faster speed for data acquisition. For testing the PDT was set to 200  $\mu$ sec, the HDT was set to 800  $\mu$ sec and the HLT was set to 300  $\mu$ sec.

Continuing under 'Hardware Setup', the next set of parameters are found under the 'Data Sets' button as seen in Figure 2-3. This is a set of fourteen user-selectable features corresponding to the typical parameters associated with an AE waveform. The typical parameters recorded for all tests are: Amplitude, Energy, Counts, Duration,

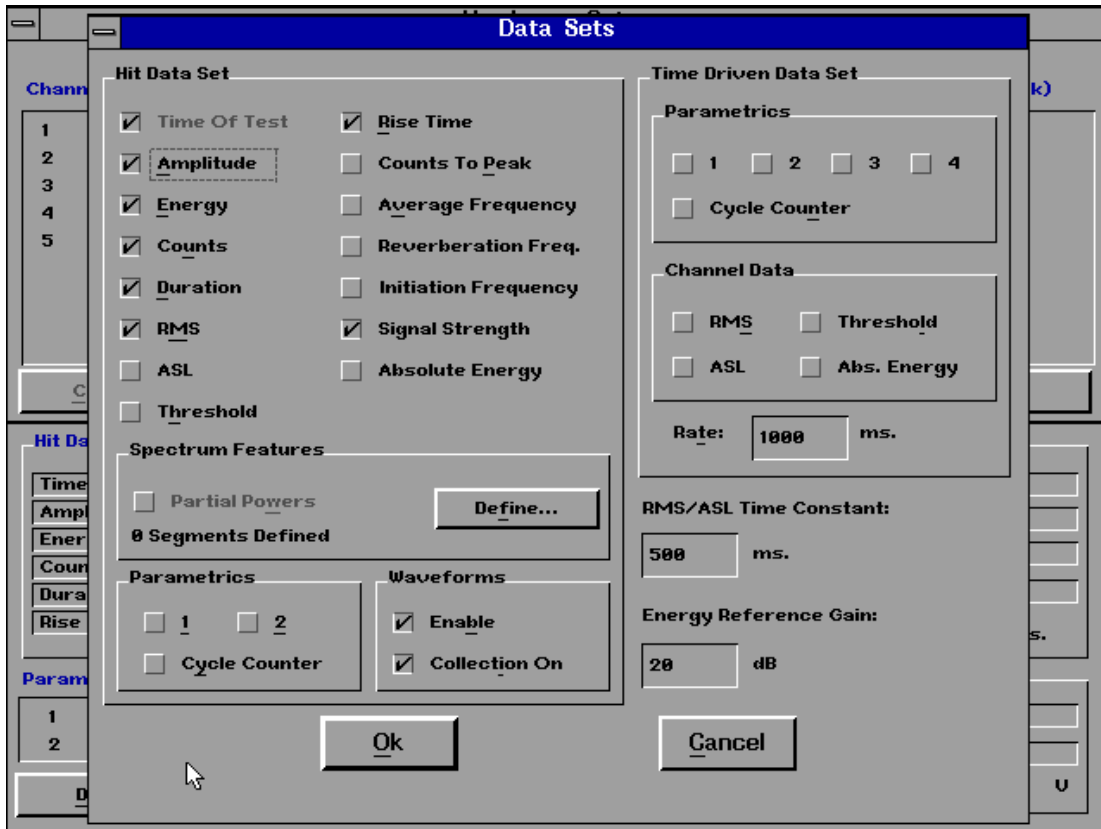


Figure 2.3: User interface for selecting data sets

RMS, Rise Time and Signal Strength. The 'amplitude' is the maximum AE voltage peak in the signal waveform, expressed in db, and expressed using the following relationship:

$$db = 20 \log (V_{\max}/1\mu\text{-volt}) - (\text{Preamplifier Gain in dB})$$

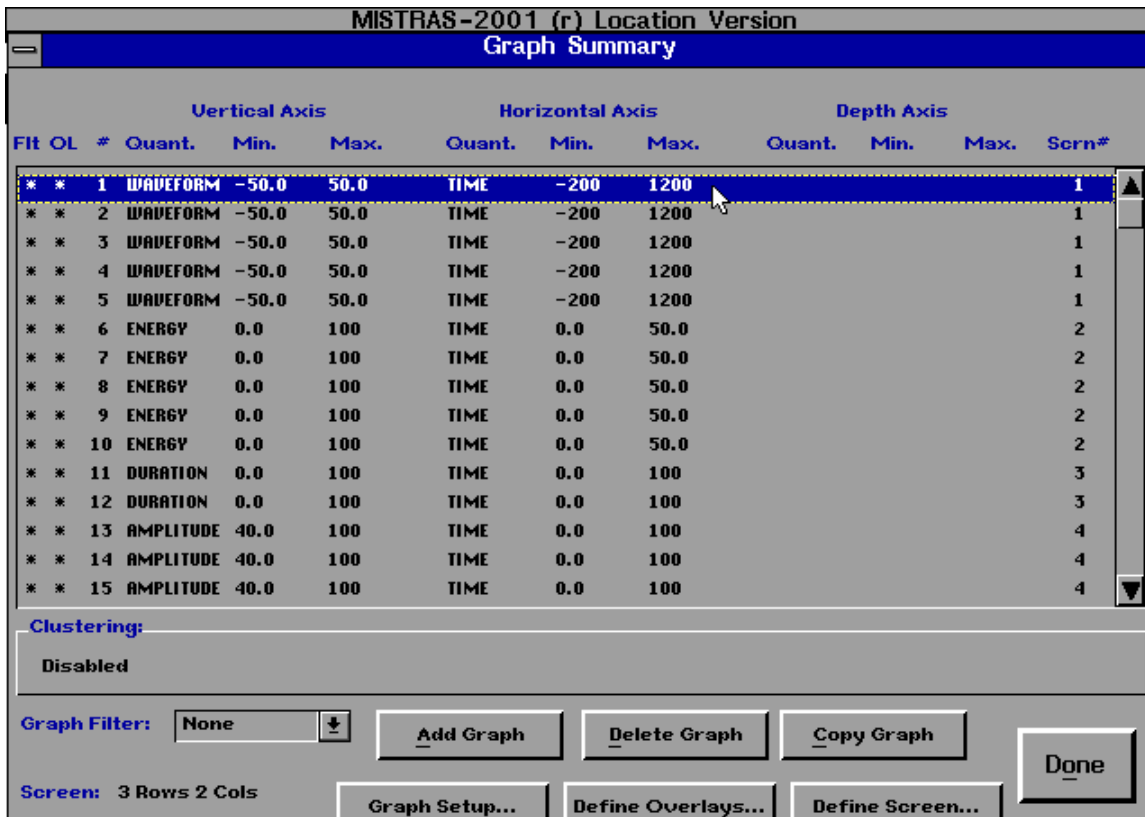


Figure 2.4: User display showing Mistras graph summary

For example, if the maximum voltage detected is 1 volt, and the pre-amp gain is 40 db, the resulting amplitude is equal to 80 db. The 'energy' is the integral of the rectified voltage signal over the duration of the waveform. 'Counts' refers to the number of times that the AE signal crosses the detection threshold. The 'duration' is the amount of time between the first and last threshold crossing. 'RMS' is the root mean square of the continuously varying voltage due to background noise in the signal. 'Rise Time' is defined as the amount of time between the first threshold crossing and the peak amplitude of the signal. In order to collect waveforms for post analysis and viewing, the user must 'Enable' and set the 'Collection On'. Otherwise, the original waveforms associated with each hit during monitoring will not be collected. Waveforms can be generated from the collected waveform parameters; however, original information contained in the waveforms will be lost (such as boundary reflections or other associated information).

After the hardware information has been configured, the next parameters to set is found in the 'Graphics' menu. Figure 2-4 provides a graph summary for the typical settings used in testing. The function of each graph is to display the data during test monitoring or replay. There were a total of nineteen graphs used during the monitoring process. The typical settings for each type of graph can be found in the Appendix A. The use of the graphs during monitoring allows the investigator to identify patterns in the data that may be useful in analysis. Once all hardware settings and graphs have

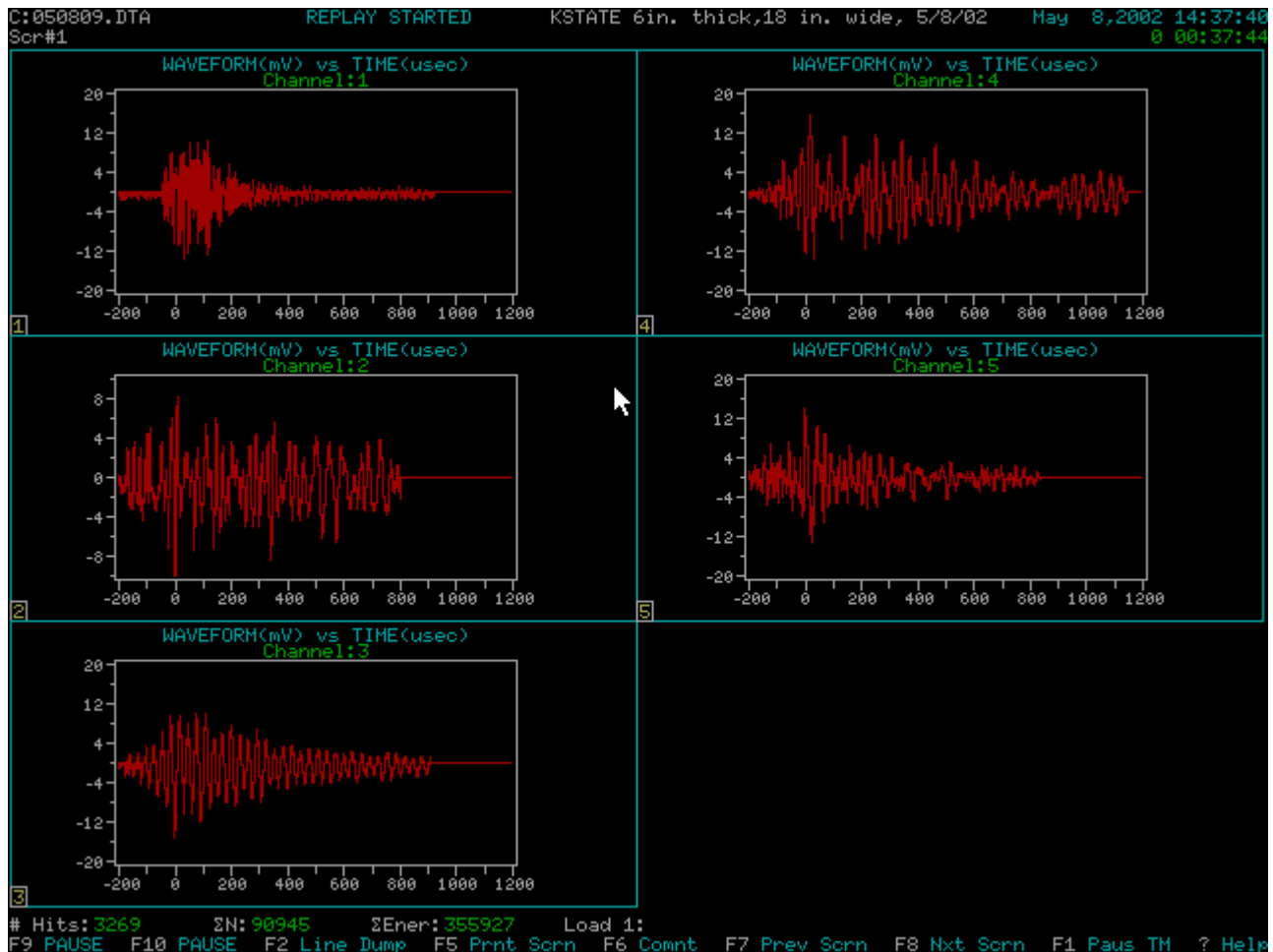


Figure 2.5: Waveform display for screen #1

been set, the information is written to an initialization file (\*.ini) so that the same setup can be used for future monitoring tests on similar specimens.

Once testing is ready to begin, the technician will go to the main menu and select 'Acquire' to begin the monitoring process. Within this menu is the technician will click on the 'Start' button which will open a dialog box for 'Test Storage'. In this window, the data 'File Name' is created (.DTA), the 'Directories' for where the file will be saved. Within this window it is critical that the checkbox for 'Autodump' is selected. This selection will then automatically write the incoming data to the file. Otherwise, no data will be written to disk and the data record will be limited to the real-time graphic view. The data file is automatically closed and reopened every 16 kbytes in order to minimize the loss of data in the event of a power failure. Once the information has been entered, the user will click on the 'OK' button to prepare the system for monitoring. The software will then switch to real-time graph mode and will display the screens setup in the graph menu. To begin testing, the technician will hit the 'Enter' key on the keyboard to start the monitoring process. The name of the file appears in the upper left-hand corner, with the date and time in the upper right-hand corner and the title in the center. In the lower left-hand side of the screen display the total number of hits, cumulative count number and cumulative energy are shown and updated regularly during a test. This information, along with the load is recorded at intervals set by the discretion of the AE technician. Figure 2-5 is an example of one the screens displaying the incoming waveforms for each individual channel. Before each monitoring test, a trial set of data is taken, using a pencil lead near each sensor (transducer) to ensure that each sensor is working properly and that the DAQ system and software are operating correctly. Once testing begins, the

F8 key will allow the technician to switch to the other graphics screen. During monitoring, attention is paid to the screens displaying waveform, amplitude versus time and cumulative signal strength versus time. In particular, the screen for cumulative signal strength versus time was determined to be a precursor for identifying the zone in which the majority of the activity is occurring. To end the monitoring process, the technician must hit the F9 key to 'Pause' the system and then F10 to 'Stop'. If this process is not followed, the system will immediately close the data file and result in the loss of data still within the buffer. Stopping the system will return the technician to the 'Main Menu'.

The concluding processes to be performed once testing is complete are accessed under the 'Utilities' menu. The first utility is the 'TIMECHK' function which analyzes the data file to determine if the data is in the correct time order and will display the number of AE messages and time driven messages. It is possible that the data may not be ordered correctly during times when a large series of events are occurring and being

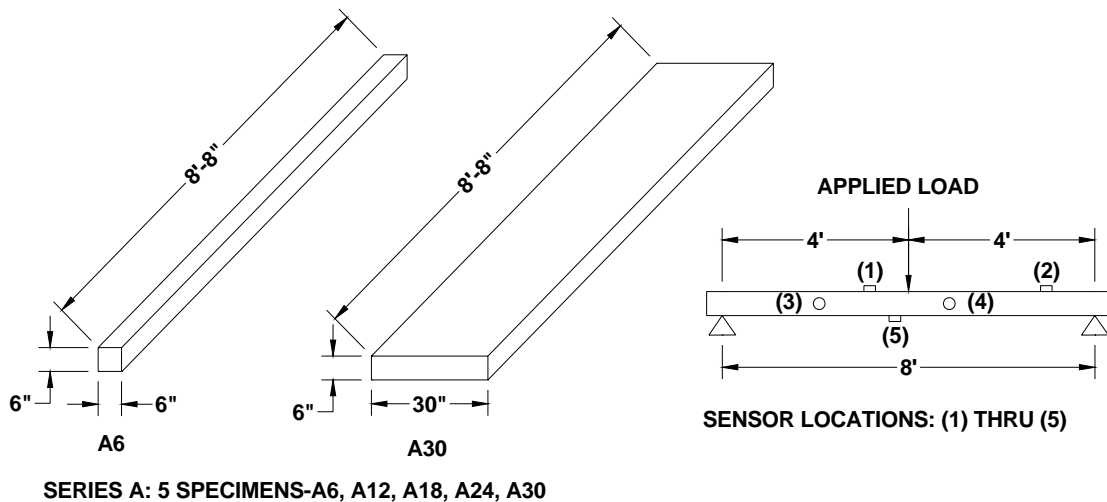


**Figure 2.6: Typical sensor locations**

recorded by the system. This is a common occurrence and is due to speed limitations of the machine and DAQ system. In the event that the data file is out of time order, the technician will need to time order the file by running the ATTO utility. This utility requires inputting the name of the original file and designating a new file name for saving the data in the correct order. Once this has been completed, if the technician plans to use the data for post processing (i.e. Excel), the ATASC needs to be run into order to convert the AE feature data from the original .DTA file into a newly created ASCII text file. Several flags may be used to configure the output. The 'beginning time' and 'ending time' flag will select a select the portion of the data of interest. The 'seconds display' flag will convert the time into a total number of seconds and fractions of a second (SSSSS.mmmuunn) from the default hour:minutes:second.fractions of a second format. Since the data file contains both hit driven and time driven data mixed together, they represent two distinct kinds of data and are in a different format. For these tests, only the hit driven (AE data) is of interest and is the default output and will not need to be changed unless time driven data is needed. This completes the setup and use of 'Mistras'.

### **2.3 AE Sensors and setup locations**

An acoustic emission sensor converts mechanical energy from the elastic wave into an electrical signal with associated waveform parameters. Thus the more correct term to be used is transducer. AE transducers contain a thin disk of piezoelectric material which converts the mechanical energy into a measurable electrical signal. A total of five sensors were used for each test. The types of sensors used for these tests included PAC R-15 resonant sensors at 150 kHz, and broadband sensors with a flat response

between 100 and 2100 kHz. Each sensor was connected (by coax cables) to a 40 db preamplifier, which is then connected by additional coax cables to a PCI-DSP4 board. A single board has up to four connectors that correspond to four channels within the software setup. Each sensor is coupled to the specimen in order to minimize energy loss between the material and sensor interface using hot melt glue and further restrained with duct tape to prevent movement or uncoupling of the sensor during testing. The typical sensor locations can be seen in Figure 2-6. Two sensors were placed on the top panel of the specimen, two on the side panel (along the core/web) and one sensor on the bottom panel, along midspan, of the specimen. All sensors were placed along or as close as possible to the centerlines, respective surface.

#### **2.4 GFRP Bridge deck panel manufacturing and specifications**

The bridge decks systems used in this study were developed by Kansas Structural Composites, Inc. (KSCI). All panels were manufactured using a hand wet lay-up process.

The specimens are designated A6, A12, A18, A24 and A30 with the number identifying the nominal width of the specimen in inches and “A” identified the series. The first two tests were on the original manufactured condition of the FRP panels and designated “original” (e.g. A24-Original). The final four tests were performed on the original panels that were loaded to failure and then repaired using an external wrap and which will be called the ‘repaired’ panels. Each specimen was tested as a simply supported three point bending test with an eight-foot span (Fig. 2-7) according to ASTM



**Figure 2.7: Sensor instrumentation of A18-repaired panel**

Standard C393-00 in order to determine the flexural properties of the sandwich panels being investigated by the K-State research team. For the purpose of AE, a special loading profile (consisting of load holds, load drops and load increases) was designed for each test. Each load hold was conducted for 3 minutes, in which the load was increased or decreased to the next load step. The load, hold, unload sequence (to previous load levels) was designed to assess AE signature characteristics such as Kaiser Effect and Felicity Ratio which are typically used in analysis. The load profiles were based upon a calculated percentage of service and ultimate load. Typically, active monitoring of the specimens included up to 70% of the estimated ultimate load. Sensors were removed before failure to prevent damage.

#### **2.4.1 Panel Manufacturing and Specifications**

The original panels consisted of two outer face panels (for flexural rigidity) and a honeycomb core (for shear). The core consisted of Chop Strand Mat (ChopSM) and consisted of alternating flat and sinusoidal plates (referred to as flats and flutes, respectively). Each flat and flute is laminated separately by placing a cured flat on top of

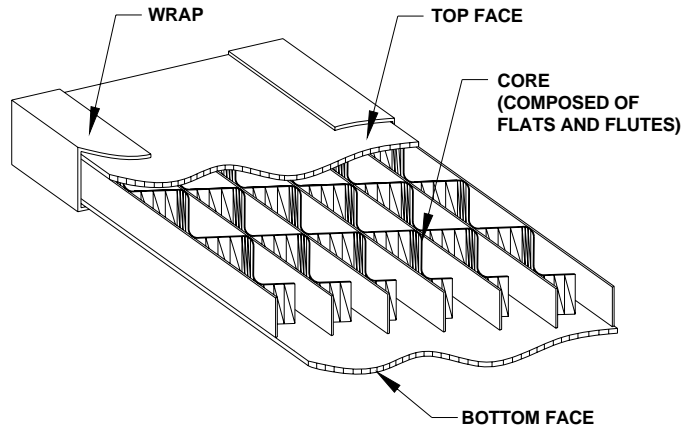


**Figure 2.8: Typical GFRP panel architecture**

a wet flute and allowed to cure. The total core is continued by using the flat to flute bonding procedure using a polyurethane adhesive (Figure 2-8). The face panels (top and bottom) are laminated by consecutively stacking resin-soaked plies on top of each other. The total core is then placed on top of the bottom face laminate while the resin is still wet and pressed into the face using dead weight. The materials are then allowed to cure and then the top face laminate is then applied to finish the panel (Fig. 2-9).

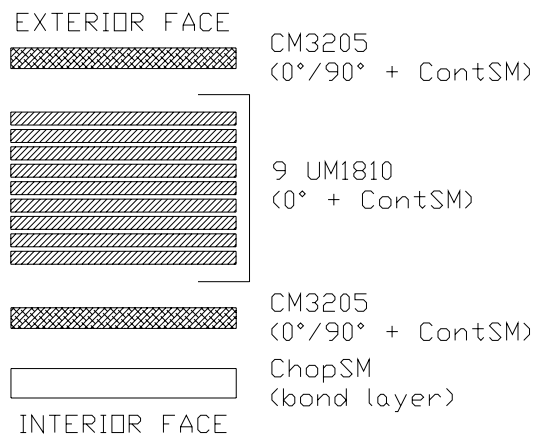


**Figure 2.9: Typical face panel architecture**

E-glass fiber mats were fabricated using four types of architecture. The different types are as follows: The face panels were fabricated as a mat using a combination of (1) bi-directional ( $0^\circ/90^\circ$ ) stitched fabric in an orthogonal direction (balanced number of

fibers) and (2) unidirectional (0°) fiberglass; the honeycomb core is a combination of alternating flat plates (flats) and sinusoidal plates (flutes). Each flat and flute is made up using (3) Chop Strand Mat (ChopSM). ChopSM uses short fibers in a random orientation. ChopSM is also used to provide a uniform bond layer between the outer face panels and the core, provide a rebonding layer for the repaired specimens which utilized an external wrap, and for the makeup of the external wrap; (4) Continuous Strand Mat (ContSM), continuously random oriented fibers, is also used to provide additional backing for other layers. The properties of the constituent materials were obtained from coupon tests performed by the K-State research group. Though these properties were not used for analysis by the researcher, the information is provided in Table 2-1 for reference.

**Table 2.1: Constituent Material Properties (for Polyester Resin)**

Property	ChopSM	Face Laminate 0° (Longitudinal direction)	Face Laminate 90° (Transverse direction)
E	1.176 Msi (8.11 GPa)	2.796 Msi (19.28 GPa)	2.180 Msi (15.03 GPa)
n	0.312	0.278	0.196
G	0.448 Msi (3.09 GPa)	— <sup>A</sup>	— <sup>A</sup>
s <sub>ult</sub>	16.3 ksi (112 MPa)	27.3 ksi (202 MPa)	16.4 ksi (113 MPa)
e <sub>ult</sub>	14.860 me	9700 me	11,000 me
t <sub>ult</sub>	0.571 ksi (3.94 MPa)	— <sup>A</sup>	— <sup>A</sup>

t<sub>ult</sub>: Ultimate interlaminar shear stress

—<sup>A</sup> : Value is not applicable or not obtained from testing

Each original specimen was loaded to failure and it was noted that the primary failure was due to flexure and occurred at the bond interface between the outer face and core. This failure mode tended to leave the face laminates and core in good

condition. Thus, for repair, the outer faces were completely removed from the core and rebounded using three additional layers of 3.0 oz. ChopSM. Then the external wrap was applied over and along the edges of the panel (Fig. 2-10).

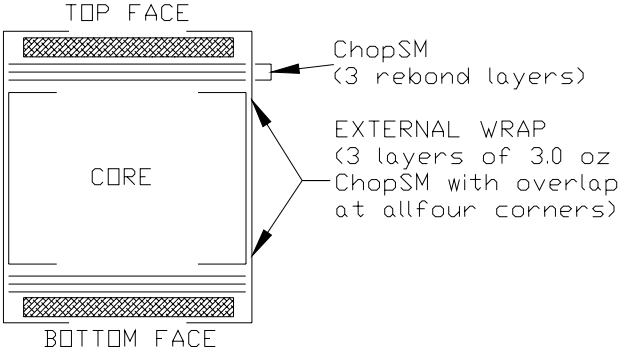


**Figure 2.10: External wrap repair modification**

No surface treatment was applied as the flexural contribution of the surface was not utilized in the design of the panels.

## CHAPTER 3 – RESULTS AND EVALUATION

This chapter presents the results from selected test cases for comparison analysis, intensity analysis and signature analysis using waveform pattern recognition techniques and neural networks. Refer to Cai Et Al. (2003) for additional information regarding the analysis and recommendations for width to depth ratio, deflection, strain and shear stress failure criteria performed by the Kansas State University research team. The selected test cases provide greater detail and comparison between the original and repaired panels.

### 3.1 Test Case: A30-Original

As discussed in Chapter 2, several screens were utilized during testing to monitor the AE activity for each channel. It was noted which channels contained the most activity in order to identify the areas of interest and focus the investigation for post analysis after testing was completed. For sensors that were located on the same

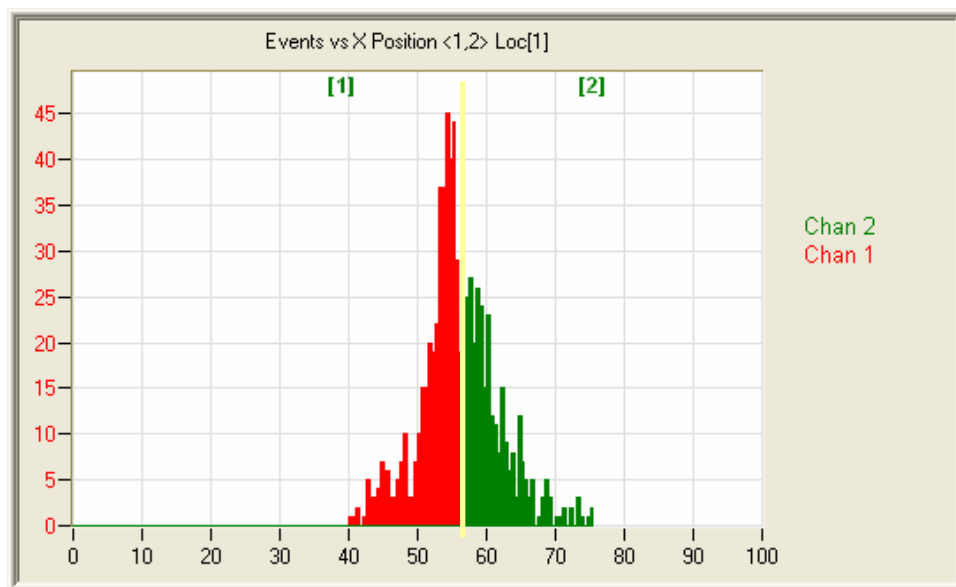
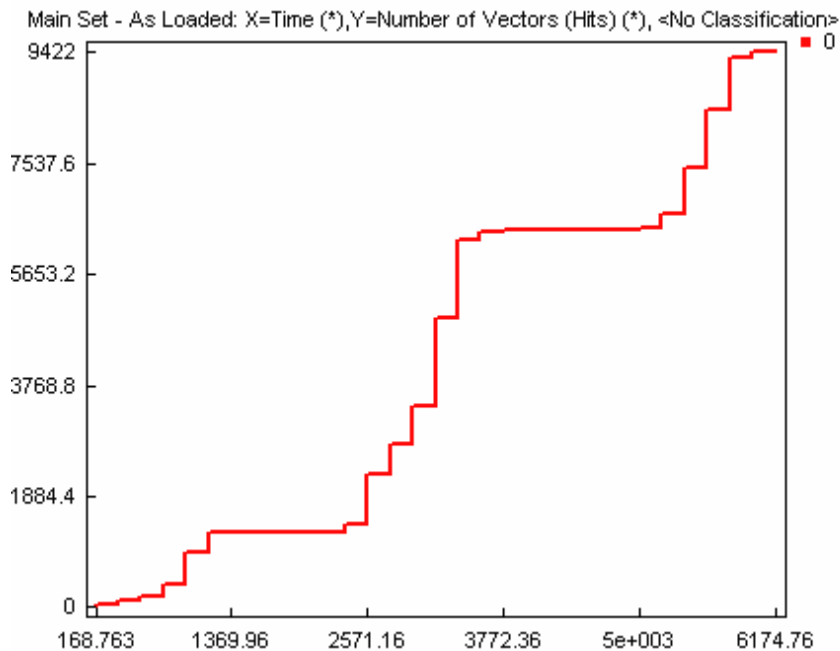


Figure 3.1: Linear location plot for A30-Original panel

surface, the built-in linear location module was used to identify the location of where the majority of the events were taking place. Specifically, a single event will generate a wave that propagates through the material and will eventually be received by both sensors and recorded as two separate hits. Based upon the calculated wave velocity (135,000 in/sec), the module determines which hits correspond to a single event, and which sensor first received the event. The module then plots the location of the event between the two sensors (Figure 3.1). As it can be seen, the majority of the events occurred to the right of the centerline of loading. The built in “replay” function allows the entire data set to be reviewed to determine the propagation sequence in which the events were recorded. For this panel, the population of the graph corresponds in time to the increase in the load and resulting deflection. An additional plot, Figure 3.2, is used to validate the propagation sequence during replay. Figure 3.2 is a cumulative plot of the A30-Original panel which displays three distinct areas in which there was an increase in the number of incoming events.



**Figure 3.2: Linear plot of cumulative hits for A30-Original panel**

This plot is useful for identifying the critical event stages during testing and can be compared to the loading sequence to determine if a correlation exists. Before comparing this graph to the loading profile, a final graph is used to separate the number of recorded hits by the channel that received them (Figure 3.3). As it can be seen the majority of the events for the A30-Original panel were recorded by channel 5 with the fewest events recorded by channel 3.

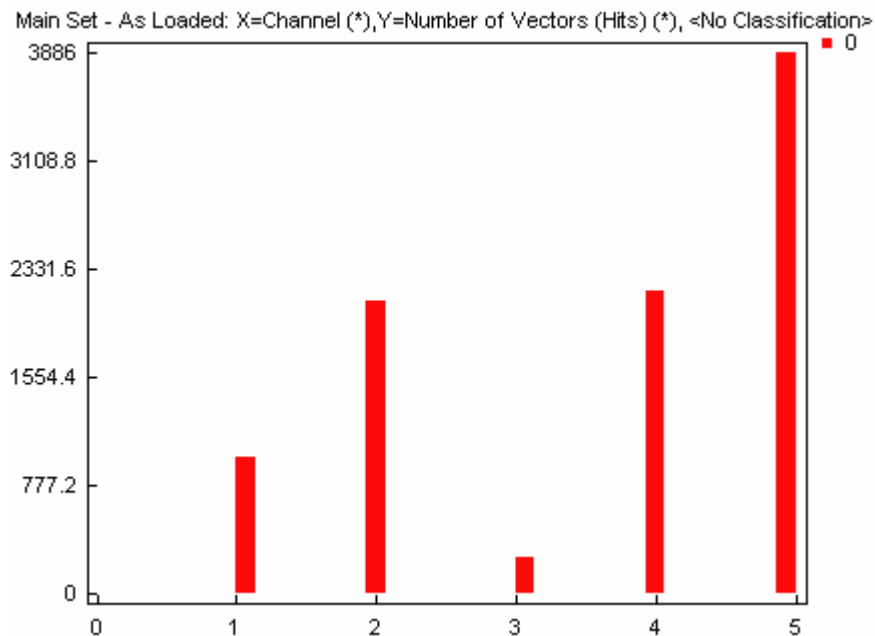


**Figure 3.3: Histogram plot of #of hits by channel**

Now that this basic information is known, the rest of the post analysis will focus on channel 5, which is the sensor located along the centerline of the bottom face panel.

### **3.1.1 Comparison Analysis**

As discussed in Section 1.4, comparison analysis allows for the correlation of the properties of the acoustic emission event using plots of duration versus amplitude, and the duration, peak amplitude, and cumulative signal strength versus time. Along with a special loading profile, this approach allows for the assessment of certain AE signatures

such as Kaiser Effect and Felicity ratio. This type of assessment is currently used as evaluation criteria of tanks and vessels (Blessing et al. 1989, CARP 1987).

The first plot used for comparison analysis is a plot of the amplitude of each event in time with the superimposed loading profile (Figure 3.4).

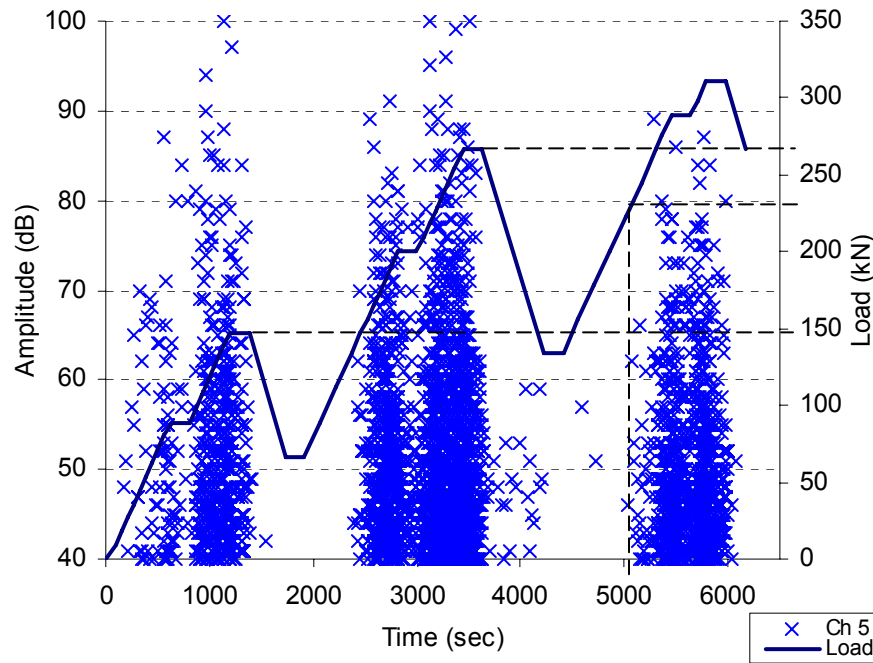


**Figure 3.4: Plot of amplitude versus time**

Figure 3.4 is the plot for the A30-Original panel. Referring to Figure 3.3, channel 5 was determined to have recorded the greatest number of hits and thus is the focus for this part of the analysis. The Kaiser Effect is a case of the indication of prior loading of a specimen. This effect states that if a sample is loaded, unloaded and then reloaded under the same conditions, no acoustic emission events should be detected until the previous load peak is achieved or passed. This condition is satisfied if no permanent damage within the specimen has occurred. There are three distinct areas on the graph representing peak amplitudes of the events during the loading cycle. The first area between the start of the test and 1400 seconds has undergone a two hold times of three

minutes (typical) at 89 kN (20 000 lbF) and a peak load of 146.85 kN (33 000 lbF), which is indicated by the first dashed, horizontal line. During the subsequent unload sequence, only one single event is recorded before reaching the third load hold at 66.75 kN (15 000 lbF). After three minutes, the second loading begins and continues to the next hold limit. As can be seen by the first dashed, vertical line, the following set of AE hits recorded do not occur until the previously held load of 146.85 kN (33 000 lbF) has been reached. This area of the graph supports the Kaiser Effect which provides confirmation that no permanent damage has yet occurred in the panel.

The second load/hold sequence begins and continues until the next previous peak load is reached at 266.9 kN (60 000 lbF). After this load hold and during the second unloading sequence, a significant amount of AE events are recorded before reaching the sixth load hold. The third load/hold sequence begins and it can be seen that the AE events begin to occur at a load below the previous maximum load. At this point, the Kaiser Effect is no longer valid, and this condition is known as the Felicity Effect. This is a point in which permanent damage may be occurring in the panel. Comparing Figure 3.4 to Figure 3.2, it can be seen that the significant increase in the number of hits provides a precursor to the point in which the Kaiser Effect is likely to break down and the first Felicity ratio can be calculated. At a load of approximately 231 kN (51 900 lbF), a calculation for the Felicity ratio is made and determined to have a value of 0.87 and occurred at 51 percent of the ultimate load. Since the sensors were removed before the end of the third peak load hold, additional Felicity ratio calculations could not be made.

However, if the data was available, the second calculation would be lower than 0.87 and would be due to the increased loading and resulting increase in permanent

damage. A Felicity ratio of one or greater can be interpreted as showing no damage in the structure since the last AE inspection. However, a decreasing FR in later inspections may be indicative of the cumulative, permanent damage and may result in the rejection and removal of the panel. Two additional plots are used to provide the distribution of the events in regards to the amplitude of each hit and the number of hits recorded during monitoring. These plots can be seen in Figure 3.5. It can be noted that the majority of the hits had an amplitude between 40 and 65 dB.

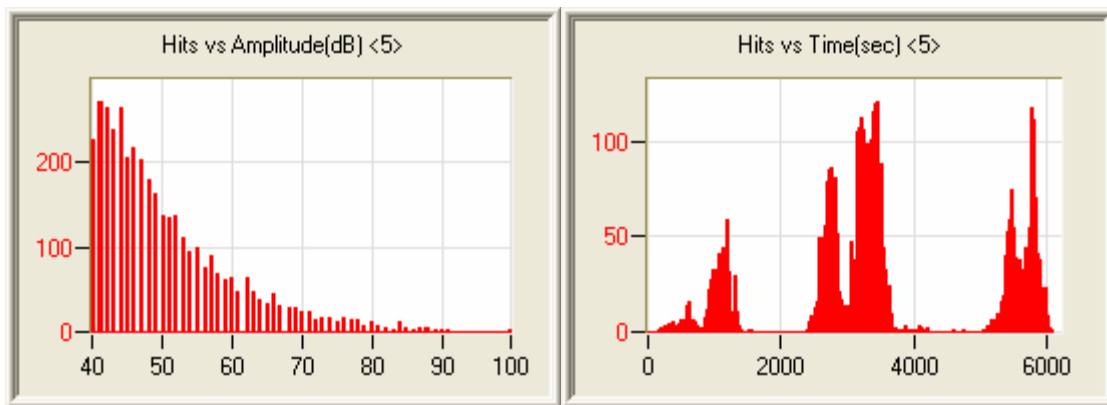


**Figure 3.5: Distribution plots of recorded hits**

The second graph used in this type of analysis is a plot of the cumulative signal strength of the events for each channel. As can be seen from Figure 3.6, channel 2 and channel 5 saw the greatest increases in the cumulative signal strength. Comparing this plot to Figures 3.2 and 3.4, this graph corresponds to what has already been seen in the previous figures.

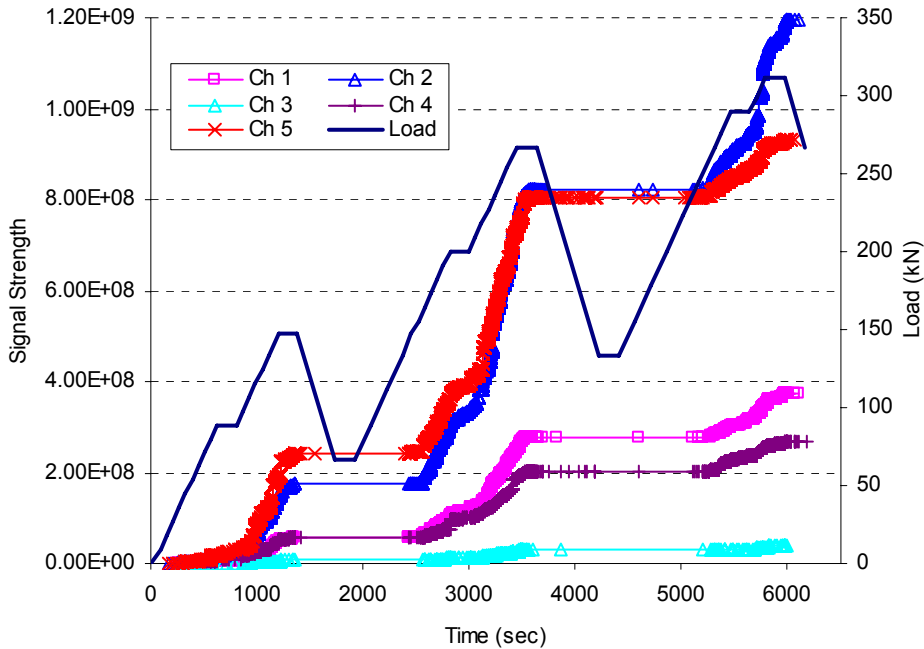


**Figure 3.6: Plot of cumulative signal strength in time for all channels**

While this information appears redundant and offers little information beyond what was obtained from the Felicity ratio calculation, it provides a check of the information contained in previously developed graphs. In this case, case it can be seen that channel 2 had a higher cumulative signal strength. However, the calculation of the Felicity ratio for this channel was higher than the calculated value for channel 5 and though AE events were recorded before the previous peak load hold, the amplitudes of the events were low and short in duration which were determined to be associated with matrix cracking.

A final comparison graph of duration versus amplitude is developed to try and characterize the events by the type of damage characteristic such as matrix cracking, fiber breakage or debonding. High amplitude, long duration events have typically shown to signify the breakage of the fibers. While events of short to medium duration and low

to medium amplitude tend to signify matrix cracking within the material and is similar to results from other work (Gudmundson, Johnson 2000) and shown in Figure 3.7.

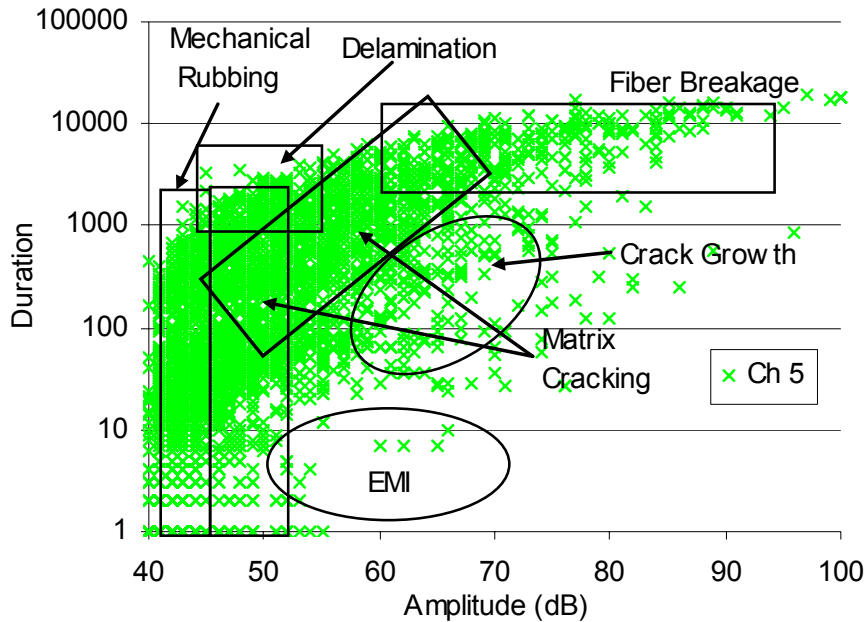


**Figure 3.7: Cross plot of duration versus amplitude**

The banded appearance is typical of for this plot and is due to an increase in amplitude and duration of the events during the monitoring process. Based on these waveform features, it is possible to create “zones” to differentiate between fiber breakage, matrix cracking, debonding or false events (AAR 1993). However, the use of this plot was limited in this analysis as many areas overlap each other and could lead to misclassification of events. It is believed, that the misclassification of events can occur because the signal wave attenuates as it travels through the material before reaching the sensor. As events occur farther away from the area of the sensor, attenuation will be greater before being recorded. Attenuation can also occur due to the absorption of the material (damping), divergence of the wave from the source point, and reflections at boundaries in which the wave will attempt to divide and redistribute the energy across

all available paths. All types of attenuation mechanisms will result in a decrease of the amplitude, duration or frequency. It is possible that an event that is classified as matrix cracking may actually be fiber breakage. Therefore, no generalizations should be made beyond the panels tested during this study.

### **3.1.2 Intensity Analysis**

To measure the structural significance of an AE event(s), intensity analysis uses signal strength to calculate two factors known as Historic Index and Severity. The HI compares the average signal strength of the last 20 events to the average signal strength of all the events. This analytical method allows for the determination of a change in slope in the cumulative signal strength curve. During initial loading, the value will be close to unity and will increase sharply at the “knee” in the curve. After the knee, the historic index will decline until the next knee is reached. Reviewing Figure 3.8 several AE knees can be seen but may not necessarily represent significance in terms of possible damage.

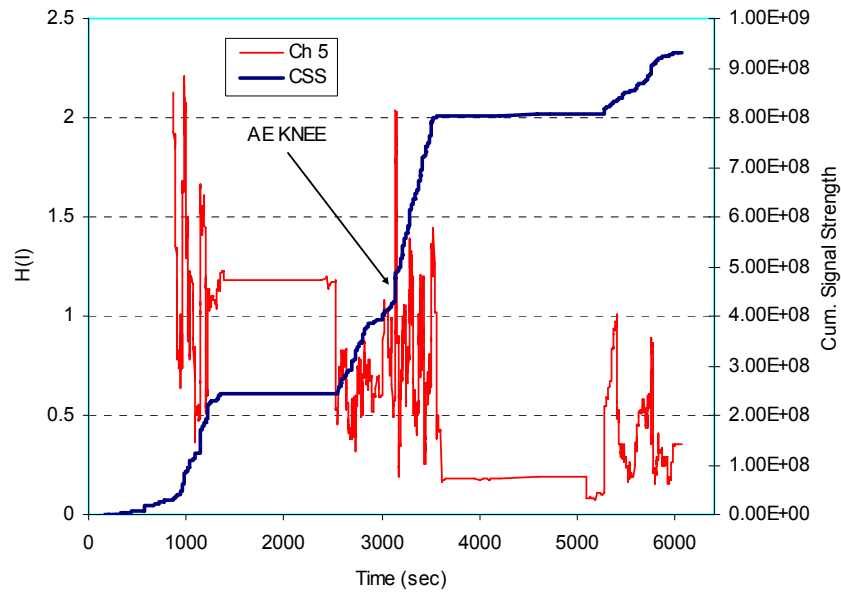


**Figure 3.8: Plot of historic index and cumulative signal strength**

For example, from the start of the initial loading sequence and approximately 1400 seconds, several peaks in the historic index value can be seen and correspond to the changes in slope of the cumulative signal strength curve. Normally, this trend is associated with the generation of high amplitude events associated with an increase in structural damage, such as fiber breakage. However, comparing this graph to Figure 3.4 in which was used to evaluate the Kaiser Effect and calculate the Felicity ratio, as previously stated, the Kaiser Effect was being observed and thus no structural damage had occurred. Thus, instead of these events being related to fiber breakage, these events were the result of gross matrix cracking, which in this case did not affect the structural integrity of the specimen. The maximum HI value during initial load was 2.21. Since matrix cracking and fiber breakage have similar characteristics, this graph helps determine which type of mechanism was being observed. This is also the reason why overlaps in events can occur in the zones as seen in Figure 3.7.

The second graph used in intensity analysis is the calculation and plot of severity with respect to time. The calculation of severity is defined as the average signal strength of the 20 events having the largest value of signal strength. In the case of severity analysis, severity can only increase with the load and a significant increase will identify the onset of increasing severity in terms of structural damage. As with historic index, severity will typically increase at the knee of the cumulate signal strength curve. As damage continues to increase in the panel, severity will increase, but at a slower rate. At the onset of more severe structural damage (such as gross fiber breakage), severity will increase sharply. These trends can be seen in Figure 3.9.

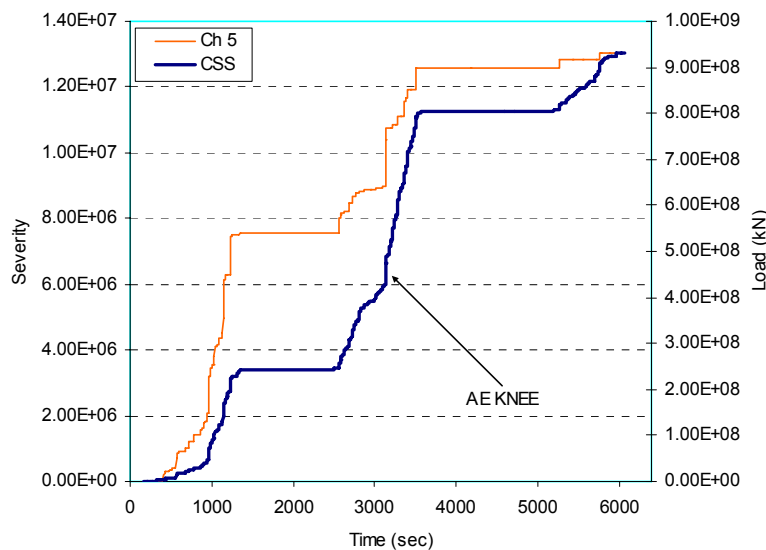


**Figure 3.9: Plot of severity versus cumulative signal strength**

Starting again during the initial loading sequence, there is a significant increase in severity that normally indicates the presence of serious structural damage. However, as previously discussed, it was determined during comparison analysis that between the start of loading and 1400 seconds, the Kaiser Effect was being observed. To better

show this relationship, Figure 3.10 shows a plot of severity with respect to the special load profile.

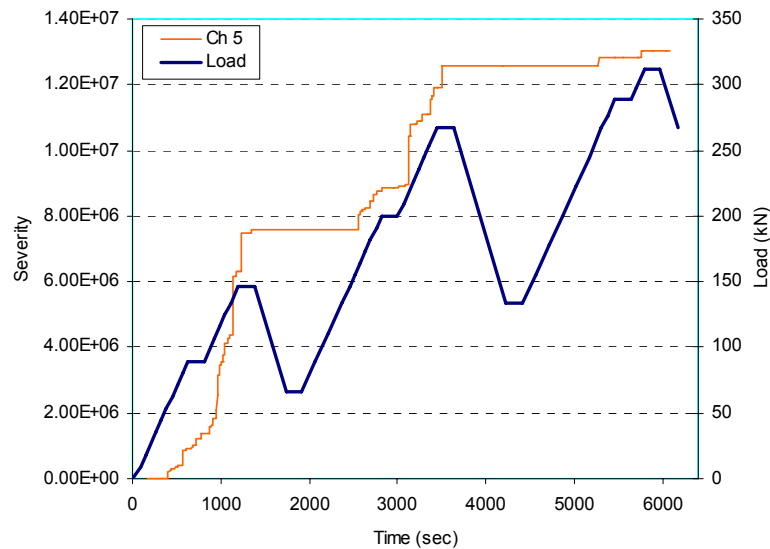


**Figure 3.10: Plot of severity versus load profile**

Notice that during the first unloading sequence, the slope of the line is zero and would correspond to no damage occurring as there is no increase in severity. During the second loading sequence, we begin to see a significant increase in severity, at a slower rate, but not until the panel had passed the previous peak load hold. This trend supports the previous analysis that the Kaiser Effect was being observed. Thus, once again, the significant rise in severity was attributed to gross matrix cracking and not fiber breakage. However, after the next unload and subsequent reloading sequence, we see an increase in severity before the previous peak load of 266.9 kN (60 000 lbF) is reached. This point in Figure 3.10 corresponds to the point at which the Felicity ratio was calculated using comparison analysis. The maximum HI value during the point at which the onset of emission was detected was 2.04. Thus the use of severity becomes

another important tool for the calculation and identification of severity for Felicity ratio calculations and is an important tool in the measure of structural damage of the panel.

Review of the analysis and corresponding data indicates that failure begins with debonding of the internal core material from the top and bottom face panels and corresponds to the activity seen on channel 5. It is believed that debonding of the core forces the load path to the outside core flats, later causing the outside flats to begin debonding from the top and bottom face panels due to the increase in horizontal shear. This load transfer and subsequent debonding corresponds to the increased activity observed on channel 2. The failure of the specimen is catastrophic and results in the specimen shattering into individual pieces (top and bottom face plates, outer flats and core). Since the failure mode was unknown at the time of testing, this resulted in the inability of the technicians to make a complete visual inspection during testing due to safety concerns. Note however, that there were no key damage indicators that could be visually verified prior to failure. A significant increase in AE emission and audible noise from the panel provided ample warning before ultimate failure occurred. The specimen failed at a load of 448.4 kN (100 810 lbf). Inspection of the panel after failure confirmed the debonding of the inner core from the face panels and the outer flats from the top and bottom face panels. No crushing of the core was observed.

The same methods using comparison and intensity analysis was performed on the remaining panels. Table 3.1 presents the results from this analysis and the associated graphs for the remaining specimens can be found in their entirety in Appendix B.

**Table 3.1: Summary of comparison analysis results for all panels**

Specimen	P <sub>max</sub>	D <sub>max</sub>	Total AE	Total AE	Felicity
	kN (lb)	cm (in)	Hits	Waveforms	Ratio
A6 - Repaired	151.1 (33 970)	5.23 (2.06)	3724	3708	0.94
A18 - Repaired	398.6 (89 580)	6.6 (2.6)	27126	25437	0.90
A24 - Original	161.0 (36 190)	3.07 (1.21)	30267	18179	0.54
A24 - Repaired	321.6 (72 260)	4.09 (1.61)	41149	28003	0.90
A30 - Original	448.6 (100 810)	6.63 (2.61)	9422	9387	0.87
A30 - Repaired	387.2 (87 000)	5.33 (2.1)	26574	15886	0.89

P<sub>max</sub>: maximum applied load before failure

D<sub>max</sub>: maximum midspan deflection

Note that the calculated FR for the A24-Original panel was 0.54. This was due to failure of the specimen occurring unexpectedly at a load of 161.0 kN (36 184 lbF). A review of the graphs for comparison analysis observed that the Kaiser effect was never observed as AE emissions were continually recorded from channel 4 during the entire loading, unloading and reloading sequence. This corresponds to a high probability that permanent damage occurred early in the testing (Figure 3.11). The Felicity ratio of 0.54 was calculated at the end of the third holding sequence of 62.3 kN (14 000 lbF). Corresponding increases in the graphs for cumulative signal strength, historic index (peak of 5.53 at a time of 920 seconds) and severity were observed. Immediately before failure, the historic index peaked at a value of 72.3 with a corresponding peak severity value of  $9.9 \times 10^8$ . Review of the analysis and corresponding data as well as a visual inspection after failure, determined that the failure was initiated along the right side of the panel (location of Ch. 4 sensor) due to debonding of the outer flute from the top and bottom face panels with subsequent debonding of the inner core. Visual inspection of the panel after failure discovered that the internal core was not fully bonded to the face

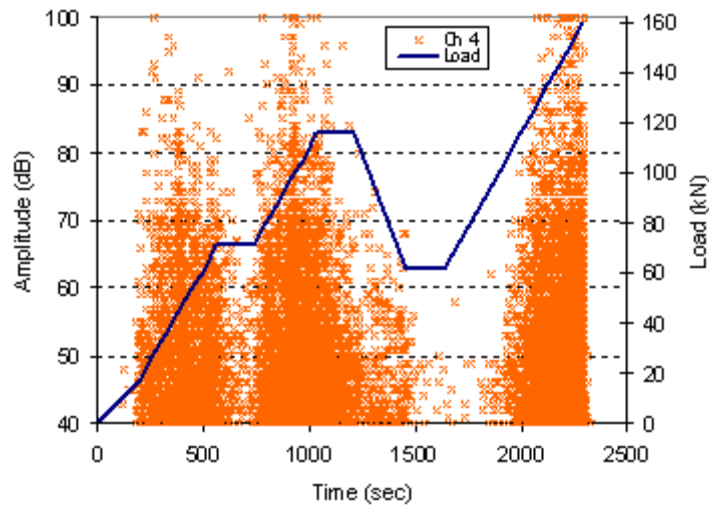


**Figure 3.11: Plot of amplitude versus time**

panels. This would have resulted in overloading of the outer flats and premature failure of the panel as the full cross sectional area would not have been available to resist the load. Thus this failure was attributed to a quality control problem during manufacturing and was not observed in any other specimen.

Additionally, the increases in emissions from the repaired specimens are believed to be associated with the 3 layer, ChopSM external wrap that is applied and bonded with resin. In the case of the A-30 repaired specimen, 63 percent of all the hits recorded were received by sensors located on the external wrap. Part of this increase in emissions is the result of mechanical rubbing of the wrap along the inner core as it begins debonding. A review of the data indicates that failure begins along the centerline of loading with the internal core material debonding from the top and bottom face plates. This forces the load path to the outside panels and into the external wrap. Once the load begins to approach the maximum tensile capacity of the wrap, or the strength of the resin bond, debonding of the external wrap tends to begin at midspan of the panel and slowly begins to expand out towards the supports. This can be seen in Figure 3.12



**Figure 3.12: Debonding of wrap along edges**

and is represented by the white areas along the top and bottom edges. This type of failure mode was observed for all of the repaired specimens. In each case, once the debonding of the wrap came to a free edge, the wrap would begin to “unzip” along the interior edge of the wrap and then shear down the outer face. Additionally, it is believed that this loading pattern contributes to the higher calculated Felicity ratios in which the points at which they were calculated normally did not occur until right before failure of the panel.

Unlike the failure mode observed with the original specimens, the externally applied wrap restricts the failure and acts as a clamp that holds the core and face panels together. This type of failure mode is preferred and presents a major advantage over the original panels. The additional advantage is that it allows an inspector to visually identify debonding failures due to a result of increased load and or damage. On top of this visual warning, the repaired specimens also provide an audible warning before failure.

### **3.1.3 Waveform signature analysis**

The final part of the study looks to identify which type of failure mechanism was being observed at the identified points in which the onset of failure was beginning to

occur and the subsequent Felicity ratios were calculated. To obtain this result, waveform signature analysis was performed in an attempt to identify each type of failure mechanism that was present.

The ability to characterize the failure mechanism into classes is important as it would provide the possibility of providing real-time monitoring characterization in which warning levels could be established for each type of failure mechanism and if exceeded, and could provide the inspector with criteria for either reducing the load rating, repairing the panel or completely removing and replacing the panel.

Since no classes have been previously defined for these panels, the A30-Original panel was used as the test model to try to develop and train a model that could be used for identifying failure mechanisms and sorting them in separable classes. If successful, this method and model could be used to evaluate new, unknown data collected from additional panels of the same manufacturing.

The original data was loaded into the Noesis software package as an unsupervised method since no classes have been identified. Therefore, the typical features loaded were amplitude, energy, duration, rise time, counts, RMS, signal strength and waveforms. Once the data is loaded, Noesis will display a default graph of the main set of data as loaded into the program. Noesis gives 10 different plot options from a simple scatter graph (Figure 3.13), to distribution, cumulative and line graphs.

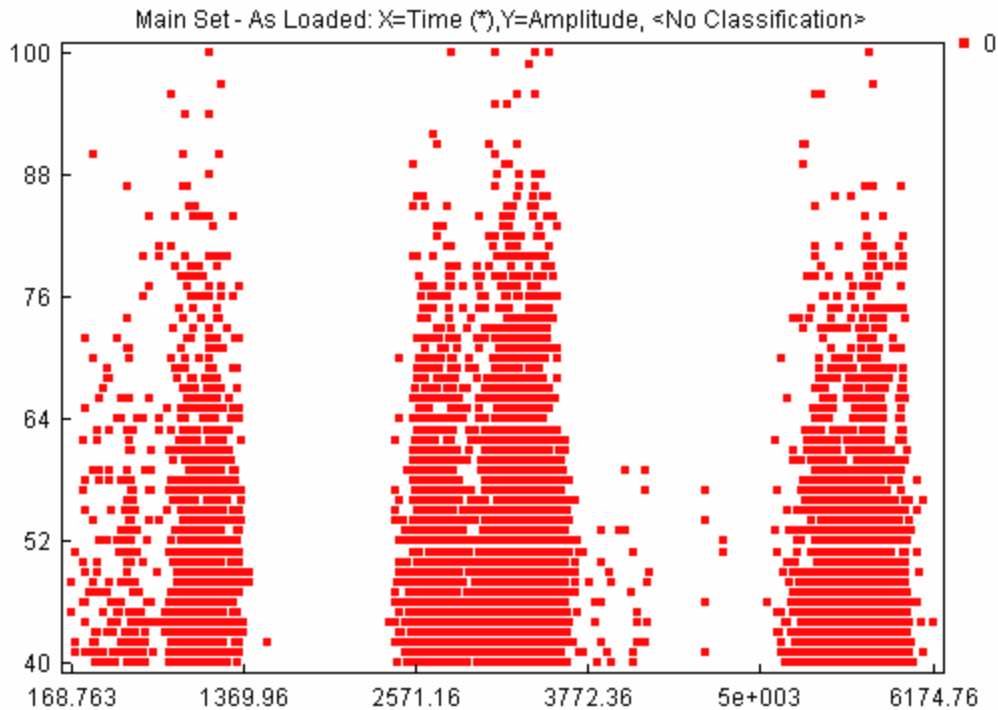


**Figure 3.13: Noesis plot of amplitude versus time**

After the initial graphs are created, additional features are extracted from the data set in order to try and identify which features will be most efficient for providing better discrimination and results between the identified classes. Feature extraction affects both the 'As loaded' and 'Working Copy' versions of the data set and allows deletion of records with no waveforms and waveforms below the set threshold. For this panel, only the waveforms below the threshold were deleted. Out of 22 additional features, 'Counts to Peak', 'Absolute Energy', 'Amplitude mV', 'Rise Angle', 'Decay Angle', 'Average Frequency', 'Initiation Frequency', 'Reverberation Frequency', 'Zero Crossings', 'FFT Amplitude', and 'FFT Peak Frequency' were added for a total of 18 waveform features.

Now that the features have been added, and channel 5 (broadband) was identified as the critical channel from comparison analysis, the data is filtered so that the analysis will only look at the data for the broadband sensors. Therefore, the data from channels

1 and 2 are filtered. This results in 32.73% of the data being filtered from the main set. To prepare the data for clustering, we switch to the 'Working Copy' data set and look at the feature correlation hierarchy for the available waveform parameters (Figure 3.14).

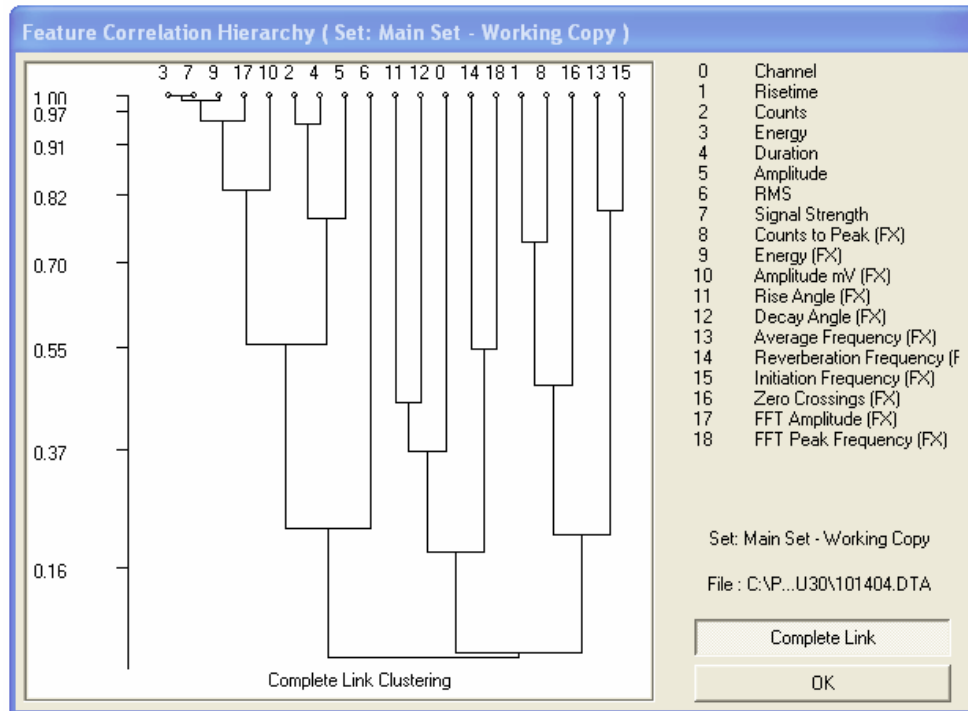


**Figure 3.14: Feature correlation hierarchy**

As can be seen from Figure 3.14, energy and signal strength have the highest correlation, followed by FFT amplitude, counts and duration and so on with channel and RMS falling in the category as the least amount of correlation between the other features. These are first results for feature identification. Based upon this correlation, energy, signal strength, FFT amplitude, counts, duration, amplitude mV, amplitude, rise time, counts to peak, average frequency and initiation frequency are chosen as the features that will be used for the first part of the analysis. Now the data needs to be normalized so that each of the selected features, which may have a different range or unit (e.g. absolute energy compared to amplitude in dB), will have the same weight.

Four different normalization schemes, 'Zero Mean', 'Unit Variance', 'Zero to One Range', and '-1 to 1 Range' are available. The '-1 to 1 Range' was used and can be seen in Figure 3.15.

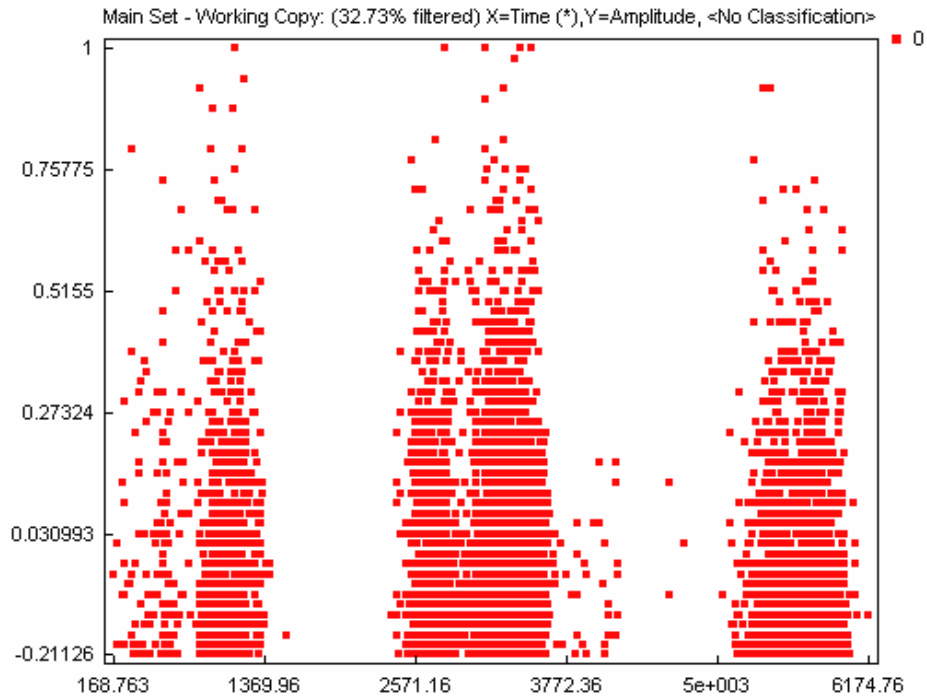


**Figure 3.15: Noesis graph with normalization applied**

With normalization applied, the next step is to project data to their principal component axes in which each axis is given a calculated eigenvalue. To further reduce the amount of features used in analysis, the correlation analysis is applied to generate new eigenvalues and further reduce the number of features for better correlation. Upon applying feature correlation, the number of features were reduced from 10 to 4 in which the highest eigenvalue was 6.264 and the lowest was 0.4945. To determine how well the new axes will fit the data, the degree-of-fit was calculated at 92.41%. Then the data selected correlation was applied and new graphs generated for each principal

component axes (Figures 3.16, 3.17, 3.18, 3.19). Each axis corresponds to a selected feature.

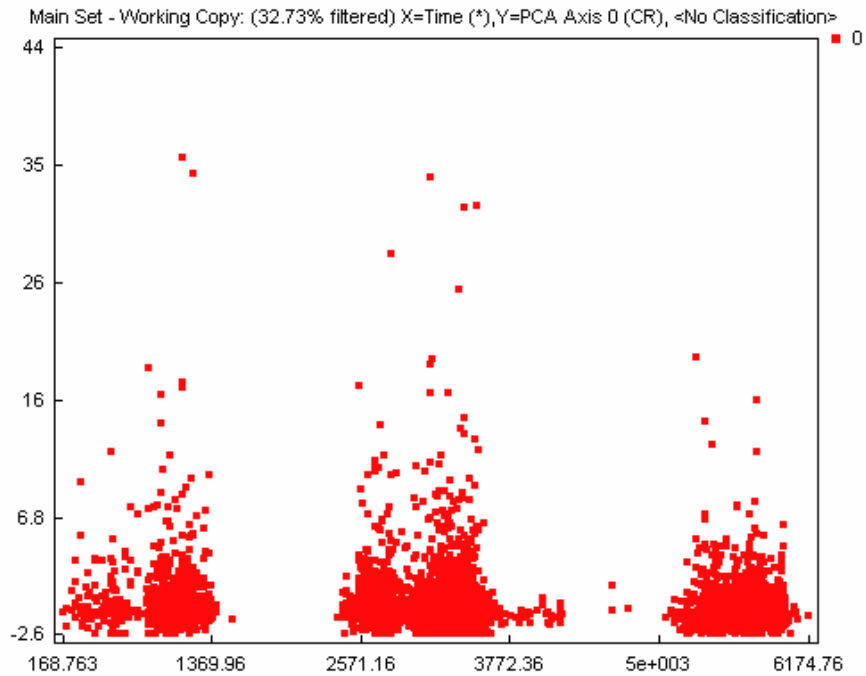


**Figure 3.16: Plot of data along PCA 0**

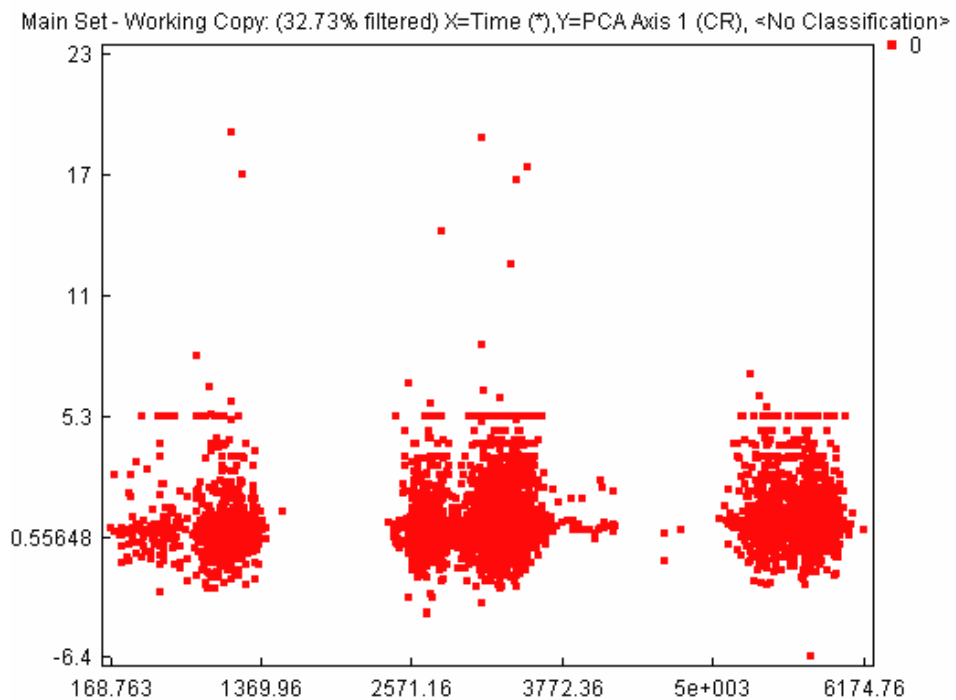


**Figure 3.17: Plot of data along PCA 1**

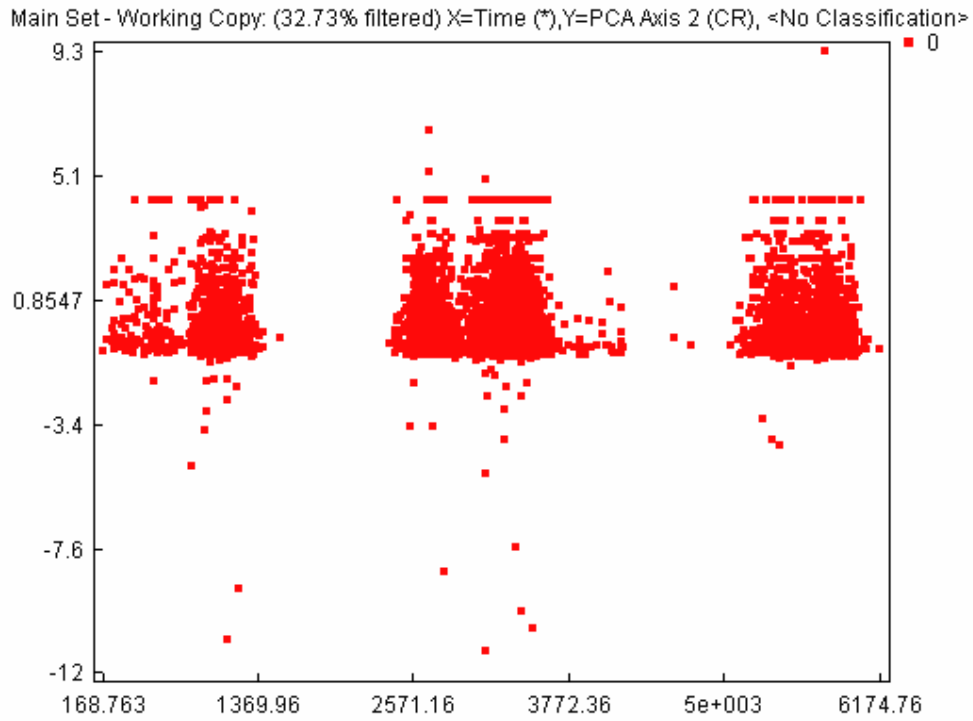


**Figure 3.18: Plot of data along PCA 2**

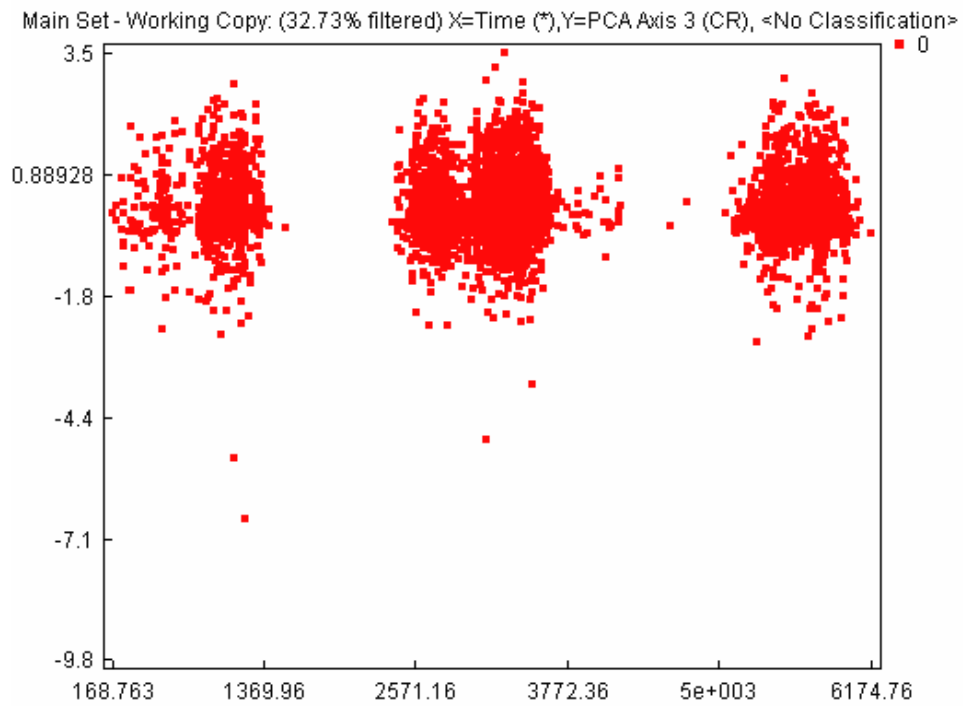


**Figure 3.19: Plot of data along PCA 3**

Now that pre-processing is complete, the data is ready for clustering. The first applied clustering technique is known as 'Cluster Seeking'. Cluster seeking is a heuristic algorithm that starts with a single point from the user defined cluster centers. A new cluster is created if a pattern is sufficiently separated, i.e. the distance between the existing cluster and the new point is greater than the specified threshold. The initial clusters were set to 6, the multiple fraction at 0.9, the minimum prototypes to 10, a radius of 0.5 and the default settings of 100 internal iterations and 20 external iterations. The multiple fraction setting is the data between the maximum radius and the percentage defined by the multiple fraction setting which will remain unclassified and are omitted from the cluster definition process. The minimum number of prototypes is the minimum number of patterns/hits in a single cluster. Clusters with fewer than the minimum number are deleted. The radius setting is the percentage of maximum distance to be used as the threshold distance for the creation of new clusters. Thus the number of clusters can be increased by decreasing the value of the radius parameter. Once all initial settings are set, the clustering technique is run. The first run using this technique generated a total of 7 classes. Each cluster was investigated by looking at the typical waveform found in the cluster to try and identify the failure mechanism within each class (Figure 3.20).

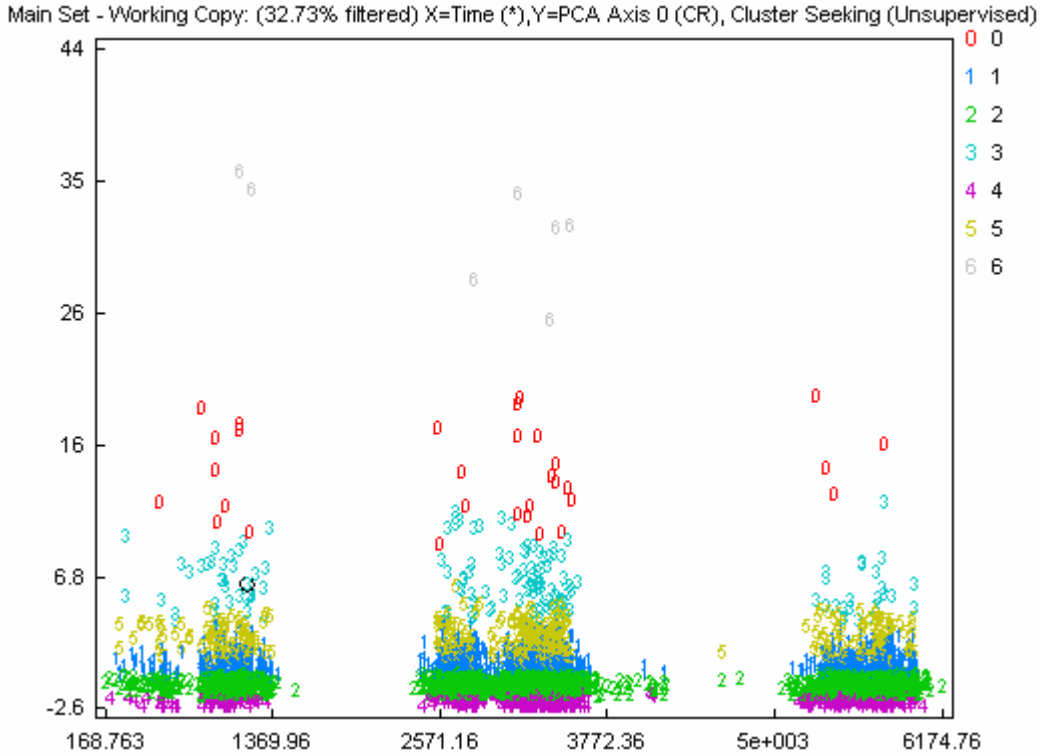


**Figure 3.20: Clustering analysis results – PCA 0**

In a review of this graph, it can be seen that the clustering technique has provided a nice separation in the data with some overlap. To gain a better understanding of the graphical representation, additional investigation reviewed the class data and feature statistics. The class data information includes corresponding centers of each cluster, sizes, inter-class distances, within-class distances and the standard deviation of each.

Table 3.2 displays the class data information from the clustering method.

**Table 3.2: Number of patterns/hits in each class**

Number of Patterns/Hits in Each Class		
<i>Class</i>	<i># of Patterns</i>	<i>Percentage</i>
Class 0	71	0.80%
Class 1	2250	23.90%
Class 2	5175	54.90%
Class 3	351	3.70%
Class 4	705	7.50%
Class 5	859	9.10%
Class 6	11	0.10%

In previous work by Gudmundson and Johnson (2000), they were able to identify waveforms that were associated with different types of failure mechanisms such as matrix cracking, delamination and fiber breakage. This work was used to try and provide an initial characterization of the waveforms within each class. For class 0 and class 6, the hits appear to be associated with individual and bundled fiber breakage. Classes 3 and 5 could be categorized as debonding or possible intra-ply delamination with classes 1 and 2 associated with matrix cracking and class 4 as possible mechanical rubbing. To try and clarify these initial characterizations, the feature statistics for each of the selected waveform features were reviewed. Features statistics contain the min, max, median, standard deviation, skewness and curtosis for each class and each feature. The combination of class data and feature statistics will allow for better clustering results and review of clusters for determination of additional patterns and identify small classes which may or may not fit with another class. Table 3.3 shows the feature statistics for each of the following classes.

**Table 3.3: Feature statistics for selected classes**

<i>Feature</i>	<b>Feature Statistics</b>			
	<i>Class</i>	<i>Min</i>	<i>Max</i>	<i>Mean</i>
1 (Rise Time)	0	25	918	343.03
	1	1	846	208.19
	2	1	651	53.71
	3	2	1296	430.45
	4	1	298	2.69
	5	8	1468	556.61
	6	48	644	201.55
2 (Counts)	0	88	409	201.75
	1	2	116	36.54
	2	1	38	5.47
	3	28	290	137.06
	4	1	3	1.02
	5	13	168	74.58
	6	255	425	312.09
3 (Energy)	0	697	2555	1334.50
	1	0	384	27.64
	2	0	24	1.86
	3	47	1015	448.69
	4	0	1	0.01
	5	8	274	91.96
	6	2352	5779	3867.90
4 (Duration)	0	2822	16285	11596.00
	1	27	5115	1498.00
	2	1	3265	264.86
	3	874	16732	7134.50
	4	1	487	3.88
	5	735	7694	3490.40
	6	12764	23599	17510.00
5 (Amplitude)	0	78	96	85.96
	1	42	89	56.00
	2	40	68	45.62
	3	66	96	74.73
	4	40	55	41.07
	5	45	79	59.41
	6	95	100	98.55
10 (Amplitude mV(FX))	0	7.7151	66.652	22.51
	1	0	27.491	0.97
	2	0	2.5361	0.22
	3	0.92776	61.525	6.32
	4	0.10071	0.54933	0.12
	5	0	9.0335	1.19
	6	57.033	99.954	86.16

Review of each feature reveals overlapping between several features and class. For instance, in looking at amplitude, class 2 and class 4 as well as class 0 and class 3 show some overlap. Recalling the previous characterization based on the waveform, the characterizations for each class is different. Thus it is possible that this approach does not always provide reliable identification of the signatures in terms of the type of damage mechanism by itself. Another possibility is that the number of features used for clustering and classification needs to be reduced in order to provide better results. Therefore, another statistical method known as 'Feature Discriminant' is used in which each feature is ranked according to their discrimination efficiency based on three evaluation criteria known as Wilk's, Rij and Tou. The calculation of each criteria value considers each feature independently. Smaller values of Wilk's or Rij indicate higher discrimination while a larger value for Tou indicates higher discrimination efficiency for each feature.

**Table 3.4: Feature discriminant analysis results**

Feature Discriminant				
<i>Ord.</i>	<i>Name</i>	<i>Wilk's</i>	<i>Rij</i>	<i>Tou</i>
1	Feature: 7(SSTR)	0.1082	1.0803	0.0021
2	Feature: 3(ENER)	0.1082	1.1426	0.0018
3	Feature: 2(CNTS)	0.1443	1.1789	0.0797
4	Feature: 4(DURA)	0.1502	1.1383	0.0887
5	Feature:17(FFTA)	0.1549	1.4557	0.0051
6	Feature:10(AMPm)	0.1812	3.9979	0.0057
7	Feature:13(AFRQ)	0.2631	84.4742	0.0001
8	Feature: 5(AMPL)	0.2833	1.8183	0.4643
9	Feature: 8(PCNT)	0.325	24.754	0.0276
10	Feature:15(IFRQ)	0.3251	7.2386	0.0044
11	Feature: 1(RISE)	0.3948	16.9742	0.0252
12	Feature:16(ZC(F)	0.5825	312.3235	0.0007
13	Feature:12(DCAN)	0.761	5.9157	0.1069
14	Feature: 6(RMS )	0.7758	53.0766	0.0063
15	Feature:11(RSAN)	0.8485	5.8606	0.1589
16	Feature: 0(CHAN)	0.9226	16.8602	0.062
17	Feature:18(FFTP)	0.9756	54.8197	0.0048
18	Feature:14(RFRQ)	0.9845	22.3534	0.0048

Using Wilk's criterion signal strength is given as the best feature to use for high discrimination of classes followed by energy, counts, duration and FFT amplitude. The same result can be seen with Rij criterion. However, Tou criterion gives the amplitude waveform feature as the highest discriminator followed by rise angle, decay angle, duration and counts. The use of duration and counts are similar for all criteria and based on this evaluation, the previous use of feature extraction during pre-processing does not appear to be useful as the additional features that were extracted do not appear to provide any assistance for defining classes and may be actually interfering with the clustering technique. Therefore, the cluster data was unloaded and the original data, using the original features, was reloaded and the same process of pre-processing and clustering was performed. This resulted in the following class data in Table 3.5.

**Table 3.5: Number of patterns/hits in each class**

<b>Number of Patterns/Hits in Each Class</b>		
<i>Class</i>	<i># of Patterns</i>	<i>Percentage</i>
Class 0	6944	73.70%
Class 1	2136	22.70%
Class 2	328	3.50%
Class 3	14	0.10%

A review of the waveforms for each class resulted in initial characterization of matrix cracking for class 0, debonding and delamination for class 1 with classes 2 and 3 being associated with individual fiber breakage and gross bundle fiber breakage respectively. Based on the review from comparison analysis, observation during monitoring and visual examination of the panel after failure, this new class structure coincides with these findings.

**Table 3.6: Feature statistics for selected classes**

<i>Feature</i>	<b>Feature Statistics</b>			
	<i>Class</i>	<i>Min</i>	<i>Max</i>	<i>Mean</i>
1 (Rise Time)	0	1	545	59.52
	1	1	1468	394.31
	2	19	1296	442.72
	3	48	644	235.36
2 (Counts)	0	1	66	8.58
	1	2	168	58.89
	2	88	409	157.45
	3	209	425	294.21
3 (Energy)	0	0	54	3.35
	1	2	368	71.00
	2	236	2018	673.59
	3	2195	5779	3551.40
4 (Duration)	0	1	3629	347.34
	1	253	7730	2712.80
	2	2822	16732	8607.40
	3	12764	23599	16613.00
5 (Amplitude)	0	40	82	46.75
	1	41	96	58.09
	2	66	96	77.57
	3	91	100	96.93

In reviewing previous work by Siron (2003), the above feature statistics in Table 3.6 are similar to their work on identification of damage and failure modes in carbon composites. Based upon their work and the findings above, the following generalizations can be made. Waveforms with low to medium amplitudes (40 to 70 dB) and low duration may represent intra-ply matrix cracking and crack propagation. Waveforms with medium amplitudes (60 to 85 dB) and medium duration may represent increased matrix cracking due to increased damage, and debonding of panel interfaces. Finally, waveforms with high amplitude (85 to 100 db) and medium to high duration may represent individual fiber failure or fiber bundle failure and large area delamination. The resulting classification and clustering technique can be seen in Figure 3.21 in which the method has been applied to the original data.

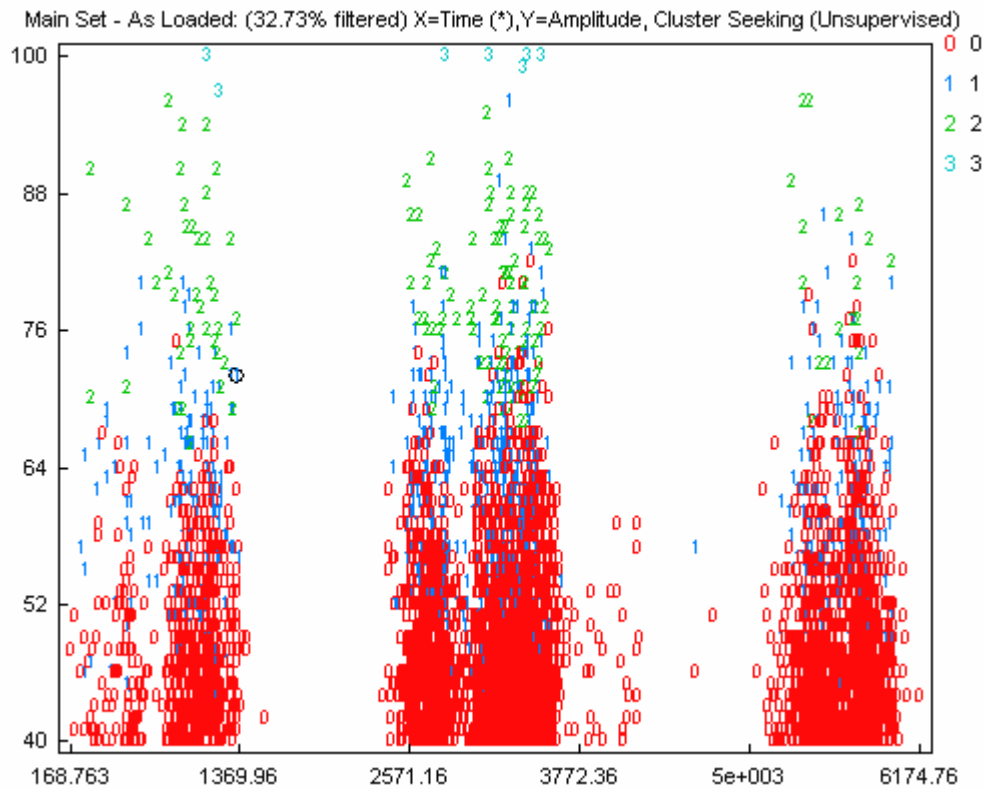


**Figure 3.21: Applied clustering method to original data**

Based on this review, this clustering method supports the initial findings. Several other available methods, such as 'Max-Min Distance', 'Forgy' and 'K-Means' were evaluated, but 'Cluster Seeking' provided the best results and discrimination. Therefore, the next step is to begin training the method for future use with other FRP composite panels. Training for the supervised method use the k-NNC method with the random half testing strategy discussed in Section 1.5. This method and strategy misclassified 38 records out of 4711 for an error of 0.81%. Based on this result the method was saved so that it can now be applied to the remaining FRP panels.

While this program demonstrates the ability to develop classes using statistical analysis and pattern recognition, the generalized classification of each damage mechanism for each class is limited to these types of specimens as the manufacturing technique used is important for understanding how the panels may have failed. Due to the lack of field experience by this researcher, a definitive methodology for in-service field inspection can not yet be made. However the use of waveform analysis presents a very powerful tool that can be built upon with more testing and experience. Another limiting factor is that the failed panels could not be obtained for micro-inspection in which failure mechanisms, such as fiber breakage and delamination, could be confirmed. The A30-Original specimen was the base model for this part of the investigation and once a satisfactory method was found, it was applied to the remaining FRP panels for comparison. The results for the remaining panels can be found in Appendix C.

## **CHAPTER 4 – SUMMARY AND CONCLUSIONS**

### **4.1 Summary**

The use of acoustic emission for monitoring and analysis of ten glass FRP bridge deck specimens were studied. The specimens varied in width and condition. Since there are no current codes or standards currently available for these particular types of specimens, current practices of evaluation and analysis for similar materials were used for comparison and validation for these specimens. Five GFRP panels were tested in their original manufactured. Each panel was monitored using AE, under a special loading profile. The failed panels were then rebonded using the original material and repaired using an externally applied FRP wrap. A total of ten panels were tested (5 original and 5 repaired).

### **4.2 Conclusions**

The following conclusions are based on the analysis and evaluation of the results of the limited study described in this report:

1. The failure mode of the original panels is sudden, and brittle. Due to safety concerns, a complete visual inspection of the original panels during testing could not be performed. This presents a safety issue that needs to be addressed. However, a significant increase in AE activity and audible cues, provided warning before failure.
2. The failure mode of the repaired specimens is preferred as the externally applied wrap acts as a clamp and prevents the panel from sudden, brittle failure. As the panel becomes distressed, the external wrap provides a visual cue of increased

damage and serves as a visual warning before failure. An increase in AE activity and audible cues also provided warning before failure.

3. There is a general increase in ultimate load capacity of the original specimens that have been loaded to failure, repaired using an externally applied wrap and reloaded.
4. The use of acoustic emission in comparison and intensity analysis allows for a check for the Kaiser Effect, the Felicity Effect, and the determination of the corresponding Felicity Ratio. This proved to be a useful tool for identification of failure criteria associated with the initiation and onset of permanent damage.
5. The Felicity ratios for the original specimens were between 0.54 and 0.87. However, the value of 0.54 was determined to be associated with a quality control problem during the manufacturing process and was not indicative of the other panels tested. The Felicity ratios for the repaired panels were between 0.89 and 0.94 and were indicative of the onset of varying degrees of permanent damage.
6. Using the wrap modification for repair adds additional noise to the panel. This increased emission becomes important for characterization of the events to differentiate between false events (e.g. mechanical rubbing of the wrap) and events associated with damage (e.g. fiber breakage, matrix cracking, and debonding). Without the ability to characterize the events, the externally applied wrap may alter the chosen point at which a value for the felicity ratio is calculated.

7. Linear location can be used to pinpoint the location of the major occurrence of events along a described axis.
8. Analyses of the waveform spectrum identified dominant frequencies of the waveforms associated with the generated events, but were not investigated to determine if they were associated with a failure mechanism.
9. The use of pattern recognition allows for general determination of classes of similar AE signals within the original and repaired specimens and identification of AE failure mechanisms.
10. FRP composites are extremely noisy and create a very large data set for analysis and classification. The majority of the data recorded was due to events generated by excessive matrix material that cracked during testing.
11. Previously established methods used in this study provide a strong foundation for developing a set of failure prediction criteria for evaluation of FRP composite bridge deck panels. However, the results from this study are preliminary and based upon a single manufacturing process and repair technique and warrants additional study.

### **4.3 Future Work**

The effects of attenuation mechanisms on the acoustic emission waveform were not evaluated in this study. Each type of mechanism, particularly boundary reflections and panel bond interfaces, will affect the properties of the waveform used to characterize an event (e.g. amplitude and duration). This could lead to possible misclassification of the event (i.e. matrix cracking versus debonding). Additional

research would provide better clarification of signal events and cleaner classification for pattern recognition.

Due to the irregular nature of the material, a higher threshold should be used during monitoring in order to provide a cleaner data set and reduce the amount of data recorded by the sensors due to excessive non-genuine events.

Since the number of specimens available for this study was limited, zonal intensity charts could not be clearly identified or established for this study. Development of these charts could provide a measure of the intensity of the events for these types of panels and would be useful for in-service field inspections. These charts could be used to identify panels with minor deterioration to those which are more severe that should either be repaired or completely replaced.

While linear location proved useful in identification of the major occurrence of events along the panel axis, additional sensors on each panel face would allow for triangular location analysis. This 2-D planar mode would provide additional coverage over a larger structure and provide better identification for the location of AE events. Additionally, once a location group has been identified, the use of guard sensors will allow the blocking of extraneous events emanating from outside a given location group.

To provide better validation of the analysis and techniques used in this study, additional research should be conducted on panels using a different manufacture and repair technique. This additional research will help identify whether or not a correlation can be made between different types of panels and already established evaluation techniques or if new criterion will need to be developed.

## REFERENCES

- FHWA. (2003). *FHWA Bridge Programs*. (n.d.). Retrieved August 8, 2003 from <http://www.fhwa.dot.gov/bridge/bripro.htm>.
- ASCE. (2003). *Report Card – ASCE* (2003). Retrieved October 10, 2003 from <http://www.asce.org/reportcard/>.
- FHWA. (2003). *TEA-21 Summary Information*. (n.d.). Retrieved August 8, 2003 from <http://www.fhwa.dot.gov/tea21/suminfo.htm>.
- FHWA, USDOT. (2002). “Corrosion Costs and Preventative Strategies in the United States” *A Supplement to Materials Performance (MP)*, NACE International, Houston, TX.(2002). Retrieved September 23, 2003 from [http://www.nace.org/nace/content/publicaffairs/images\\_cocorr/ccsupp.pdf](http://www.nace.org/nace/content/publicaffairs/images_cocorr/ccsupp.pdf) .
- Tang, Benjamin M. (2003).”FRP Composites Technology Brings Advantages to the American Bridge Building Industry”. *The Second International Workshop on Structural Composites for Infrastructure*, Cairo, Egypt.
- FHWA. (2003). Innovative Bridge Research & Construction Program. Retrieved December 13, 2003 from <http://ibrc.fhwa.dot.gov/resources/database.htm>.
- FHWA, USDOT. (1997). “Advanced Composites in Europe and Japan,” *Scanning Program Report*, Federal Highway Administration.
- FHWA. (2003). “Completed FRP Deck Projects” (n.d.). Retrieved November 3, 2003 from <http://www.fhwa.dot.gov/bridge/frp/deckproj.htm>
- FHWA/NY. (2000). “Load Testing of an FRP Bridge Deck on a Truss Bridge”, *SR-137 NYSDOT -Transportation Research and Development Bureau – Recent Research*

Reports: 1999-2001. Retrieved December 15, 2003 from  
[http://www.dot.state.ny.us/tech\\_serv/trdb/r\\_reports.html](http://www.dot.state.ny.us/tech_serv/trdb/r_reports.html)

TRB. (2003). "Committee Research Problem Statements", A2C07 Committee on Structural Fiber Reinforced Composites. Retrieved August 28, 2003 from  
[http://www4.trb.org/trb/onlinepubs.nsf/web/problem\\_statements?OpenDocument](http://www4.trb.org/trb/onlinepubs.nsf/web/problem_statements?OpenDocument)

CARP. (1983). "Recommended Practice For Acoustic Emission Testing of Fiberglass Reinforced Plastic Piping Systems". *First International Symposium on Acoustic Emission from Reinforced Composites*, San Francisco, Society of the Plastics Industry, Inc., New York.

Blessing, J. A., and Conlisk, P. J., Fowler, T. J. (1989). "New Directions in Testing", *Keynote Address, Proceedings, Third International Symposium on Acoustic Emission from Composite Materials*, Paris, France, The American Society for Nondestructive Testing, Columbus, OH.

ASME. (1985). "Standard Practice for Acoustic Emission Examination of Fiberglass Reinforced Plastic Resin (RP) Tanks/Vessels", American Society for Testing Materials, E1067-85, Philadelphia. Last revised 1996.

ASTM. (1985). "Standard Test Method for Acoustic Emission for Insulated Aerial Personnel Devices", American Society for Testing Materials, F914-85, Philadelphia.

ASTM. (1986). "Standard Practice for Acoustic Emission Examination of Reinforced Thermosetting Resin Pipe(RTRP)", American Society for Testing Materials, E1118-86, Philadelphia. Last revised 1995.

ASME. (1985). "Acoustic Emission Examination of Fiber-Reinforced Plastic Vessels", Article 11, Subsection A, Section V, Boiler and Pressure Vessel Code, American Society of Mechanical Engineers, New York.

ASME. (1988). "Fiber Reinforced Plastic Pressure Vessels", Section X, Boiler and Pressure Vessel Code, American Society of Mechanical Engineers, New York. 1988 Addenda.

Blessing, James A., Conlisk, Peter J., Fowler, T.J., and Swanson, Terry L. (1989). "The MONPAC System". *Journal of Acoustic Emission*, Vol. 8, No. 3, July-Sept.

AAR. (1993). "Procedure for Acoustic Emission Evaluation of Tank Cars and IM-101 Tanks". *Association of American Railroads, Operations, and Maintenance Department*, Mechanical Division, Washington, D.C., Issue 4, December 1993.

Fowler, T. J. (1993). "Structural Integrity Testing of Process Industry Piping with Acoustic Emission". *First International Symposium of Process Industry Piping*, Orlando, Florida, National Association of Corrosion Engineers, Houston, Texas, December 1993.

Bray, Don E., Stanley, Roderick K. (1997). *Nondestructive Evaluation: A Tool in Design, Manufacturing, and Service*, Revised Edition, CRC Press, Inc. Boca Raton, Florida.

Blessing, J. A., Fowler, T. J., and Strauser, F. E. (1992). "Intensity Analysis", *Proceedings, Fourth International Symposium on Acoustic Emission from Composite Materials*, Seattle, WA, The American Society for Nondestructive Testing, Columbus, OH

Ohtsu, M. and Ono, K. (1987). "Pattern Recognition Analysis of Acoustic Emission from Unidirectional Carbon Fiber-Epoxy Composites by using Autoregressive Modeling", *Journal of Acoustic Emission*, V.6, No.1.

Heiple, C. R., and Carpenter, S. H. Acoustic Emission Produced by Deformation of Metals and Alloys-A Review: Part I. *Journal of Acoustic Emission*, Vol. 6, No. 3, 1987, pp. 177-237.

Cai, C.S., Kalny, O., Meggers, D., Peterman, R.J., and Ramirez, G. (2003).  
“Experimental Testing of FRP Honeycomb Sandwich Panels”, *82<sup>nd</sup> Transportation  
Research Board (TRB) Annual Meeting*, Washington, D.C.

Gudmundson, P., and Johnson, M. (2000). “Transient Recording and Analysis of  
Acoustic Emission Events Resulting from Damage Evolution in Composite  
Laminates”. *Proceedings, 15<sup>th</sup> World Conference on Non-Destructive Testing*, Rome  
Italy.

Siron, O. (2001). “Identification of Damage and Failure Modes of Carbon/Carbon  
Composites Using the Acoustic Emission Technique”, *National Institute of Materials  
and Chemical Research*, AIST, MITI, Japan.

# K - TRAN

KANSAS TRANSPORTATION RESEARCH  
AND  
NEW - DEVELOPMENTS PROGRAM



A COOPERATIVE TRANSPORTATION RESEARCH PROGRAM BETWEEN:

KANSAS DEPARTMENT OF TRANSPORTATION



THE UNIVERSITY OF KANSAS



KANSAS STATE UNIVERSITY

